

Water Resources Research

RESEARCH ARTICLE

10.1002/2015WR018457

Key Points:

- Energy-balance model used to compute coastal freshwater discharge and glacier mass balance
- Results from four climate products compared side-by-side with GRACE water storage data
- Mean annual runoff from CFSR-driven runs was $760 \text{ km}^3 \text{ yr}^{-1}$, 8% from glacier volume loss

Correspondence to:

J. P. Beamer,
beamerj@oregonstate.edu

Citation:

Beamer, J. P., D. F. Hill, A. Arendt, and G. E. Liston (2016), High-resolution modeling of coastal freshwater discharge and glacier mass balance in the Gulf of Alaska watershed, *Water Resour. Res.*, 52, 3888–3909, doi:10.1002/2015WR018457.

Received 4 DEC 2015

Accepted 24 APR 2016

Accepted article online 27 APR 2016

Published online 22 MAY 2016

High-resolution modeling of coastal freshwater discharge and glacier mass balance in the Gulf of Alaska watershed

J. P. Beamer¹, D. F. Hill², A. Arendt³, and G. E. Liston⁴

¹Water Resources Engineering, Oregon State University, Corvallis, Oregon, USA, ²School of Civil and Construction Engineering, Oregon State University, Corvallis, Oregon, USA, ³Polar Science Center, Applied Physics Laboratory, University of Washington, Seattle, Washington, USA, ⁴Cooperative Institute for Research in the Atmosphere, Colorado State University, Fort Collins, Colorado, USA

Abstract A comprehensive study of the Gulf of Alaska (GOA) drainage basin was carried out to improve understanding of the coastal freshwater discharge (FWD) and glacier volume loss (GVL). Hydrologic processes during the period 1980–2014 were modeled using a suite of physically based, spatially distributed weather, energy-balance snow/ice melt, soil water balance, and runoff routing models at a high-resolution (1 km horizontal grid; daily time step). Meteorological forcing was provided by the North American Regional Reanalysis (NARR), Modern Era Retrospective Analysis for Research and Applications (MERRA), and Climate Forecast System Reanalysis (CFSR) data sets. Streamflow and glacier mass balance modeled using MERRA and CFSR compared well with observations in four watersheds used for calibration in the study domain. However, only CFSR produced regional seasonal and long-term trends in water balance that compared favorably with independent Gravity Recovery and Climate Experiment (GRACE) and airborne altimetry data. Mean annual runoff using CFSR was $760 \text{ km}^3 \text{ yr}^{-1}$, 8% of which was derived from the long-term removal of stored water from glaciers (glacier volume loss). The annual runoff from CFSR was partitioned into 63% snowmelt, 17% glacier ice melt, and 20% rainfall. Glacier runoff, taken as the sum of rainfall, snow, and ice melt occurring each season on glacier surfaces, was 38% of the total seasonal runoff, with the remaining runoff sourced from nonglacier surfaces. Our simulations suggest that existing GRACE solutions, previously reported to represent glacier mass balance alone, are actually measuring the full water budget of land and ice surfaces.

1. Introduction

The southern coastline of Alaska and northwestern Canada spanning the Gulf of Alaska (GOA; Figure 1a) is unique due to the rapid transition from marine estuaries and fjords to temperate rainforests to high mountain ranges over relatively short distances from the coast [O'Neal *et al.*, 2015]. Steep topography and a coastal marine climate combine to produce extreme rates of precipitation and the formation of extensive glaciers. Rainfall and the melting of snow and ice have been estimated to generate an average freshwater flux of $850 \pm 120 \text{ km}^3 \text{ water equivalent (w.eq.) yr}^{-1}$ [Hill *et al.*, 2015], with 7% from glacier volume loss (GVL). This flux into the GOA has strong effects on local [Etherington *et al.*, 2007] and regional [Weingartner *et al.*, 2005] oceanography. The timing and magnitude of this freshwater flux is likely to change under climate warming scenarios due to enhanced snow and ice melting [Radić and Hock, 2013], changes to the snow/rain fraction and possible changes to future rates of precipitation.

A more complete understanding of the hydrologic budget, and its sensitivity to these changes, in the GOA and in coastal mountain environments is valuable in terms of water quality and water quantity. Regarding water quality, runoff from glaciers and seasonal snow is an important control on the physicochemical properties of freshwater and nearshore marine ecosystems along the GOA. From a physical standpoint, glaciers and snow cover strongly influence summer stream temperatures [Fellman *et al.*, 2014] and thus the timing of salmon spawning [Lisi *et al.*, 2013] in coastal watersheds. From a biogeochemical standpoint, discharge from glaciers has been shown to be an important source of bioavailable carbon for heterotrophic microorganisms in rivers [Fellman *et al.*, 2015; Singer *et al.*, 2012] and nearshore marine ecosystems [Fellman *et al.*, 2010; Hood and Berner, 2009]. Regarding water quantity, many previous studies [e.g., Wang *et al.*, 2004] have omitted evapotranspiration, likely overestimating coastal runoff. In addition, most previous studies

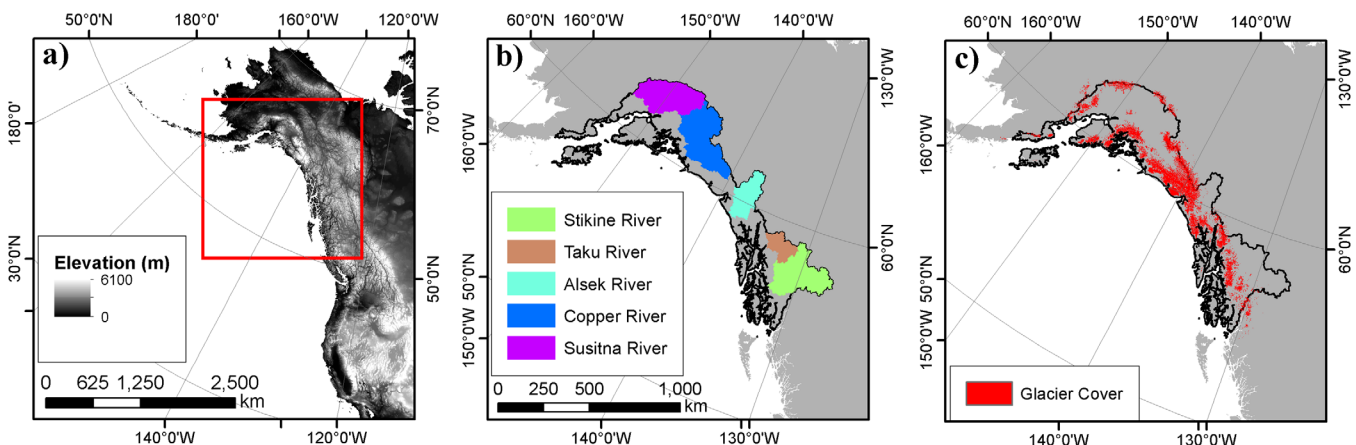


Figure 1. (a) Site map of northeastern Pacific Ocean with thick red line indicated extent of other plots; (b) Gulf of Alaska (GOA) and major inland drainage basins; and (c) glacier cover clipped to GOA domain.

have been able to capture only seasonal and interannual variation in discharge, effectively low-pass filtering the runoff hydrograph to the coast.

Several previous studies have focused on quantifying the water balance of the total GOA watershed [Royer, 1982; Wang *et al.*, 2004; Neal *et al.*, 2010; Hill *et al.*, 2015]. Although there are considerable differences in resolution and design of these studies, all predict similar mean annual GOA runoff values ($700\text{--}900 \text{ km}^3 \text{ w.eq. yr}^{-1}$) during the period 1961–2009. However, little to no attention was paid to the watershed-scale physical processes that control the release of water from storage in snowpack and glaciers, and the partitioning of rainfall and meltwater into evapotranspiration (ET) and runoff (snow melt, ice melt, and rainfall runoff).

The current study applies a distributed hydrological modeling system to the GOA watershed and distinguishes itself from previous efforts in several important ways. First, regarding modeled processes, a physically based gridded energy-balance model is used to melt the snowpack and glacier ice, providing insight into interannual fluctuations in glacier runoff. Additionally, the modeling system is modified to account for ET and soil moisture from nonglacier land surface and water bodies. As a result, it is now possible to partition hydrologic fluxes in terms of inputs (rainfall, snowmelt, ice melt) and outputs (coastal runoff, ET, sublimation). This ability to partition water sources in this mountainous ecosystem is critical for predicting both physical and biophysical changes in downstream aquatic ecosystems. Second, this study carefully considers the impact of variability in the weather forcing data on model output. Previous efforts have considered only a single weather product and the selected product has varied among studies, making direct comparisons of results problematic. Here we use four different reanalysis weather input products and investigate the resulting variability in the modeled hydrological budget. Third, this study utilizes a wide range of validation data, including glacier mass balance, streamflow, and remote sensing data, to assess performance of model and meteorological forcing data sets. Most previous studies [e.g., Wang *et al.*, 2004] used only streamflow as a performance metric that may mask offsetting model errors.

Finally, this study provides significant insight into methods for utilizing gravimetric measurements to assess hydrological changes in mountain environments. We compare model simulations of regional water storage changes generated by glaciers and snowpack to data from the National Aeronautics and Space Administration (NASA)/German Aerospace Center (DLR) Gravity Recovery and Climate Experiment (GRACE) high-resolution mascon solutions [Luthcke *et al.*, 2013]. The highly distributed nature of the energy-balance model used in this study allows analysis of water fluxes and storage changes on both glacier and nonglacier surfaces. We use this to assess the extent to which previous GRACE studies have been able to isolate glacier hydrology from other seasonally varying signals, and we use this to provide a roadmap for improved interpretation of GRACE data for assessing the hydrology of the GOA region.

2. Study Area

The GOA drainage basin shown in Figure 1b was delineated from the GTOPO (Global 30 Arc-Second Elevation) digital elevation model with the coastal boundary running from the Alaska-Canadian border to Wide

Bay on the Alaska Peninsula. This drainage contains hydrologic unit 4 (HUC4) 1901 (Southeast Alaska) and 1902 (Southcentral Alaska) from the national hydrography data set (NHD) along with portions of western Canada, and has a total area of 420,300 km². The elevation ranges from sea level to 6200 m, and four major mountain ranges broadly define the landscape. The Alaska-Aleutian Range forms the western and northern edge, the Chugach Mountains form a rim near the central coast, and the Wrangell Mountains lie northeast of the Chugach Range and south of the Alaska Range. The Chugach and Wrangell ranges merge with the St. Elias Mountains, extending southeast through Canada and the Alaska panhandle as the Coast Range. The land cover in the GOA basin is a mixture of forests (30%), grassland/shrub (27%), bare soil/rock (18%), permanent snow/ice (17%), and lakes/wetlands (8%), based on the North American Land Change Monitoring System (NALCMS) land cover map (<http://landcover.usgs.gov/nalcms.php>, last accessed 13 October 2014).

The complex topography of the GOA basin is matched by a complex mix of climate zones [Bieniek *et al.*, 2012], ranging from a maritime region, which includes southeastern Alaska, the south coast, and southwestern islands; a continental zone in the interior basin areas; and a transition zone between the maritime and continental zones that includes the southern portion of the Copper River watershed, the Cook Inlet area, and the northern extremes of the south coast area. The high mountains (elevations >4 km) along the GOA coastline coupled with abundant moisture produce precipitation amounts in excess of 12 m w.eq. yr⁻¹ in the southeastern panhandle, and averaging 2.0 m w.eq. yr⁻¹, arriving primarily in autumn and winter as snow [McAfee *et al.*, 2013]. Bieniek *et al.* [2014] analyzed divisional and statewide changes in air temperature and precipitation for Alaska from 1949 to 2012. During this time period, the statewide mean annual air temperature increased by 1.7°C, with strongest warming in the winter (3.7°C). Changes in precipitation were less obvious due to geographical and seasonal heterogeneity, but their findings indicated an increase in precipitation in the southern coastal divisions in autumn and winter, with decreases in the spring months.

Abundant snow accumulation has created a dense network of glaciers in the GOA watershed (Figure 1c) with an area of 72,302 km² of which tidewater and lake/river terminating glaciers comprise 13% and 19% of the total glacier area, respectively [Pfeffer *et al.*, 2014]. Despite the potential for rapid dynamic ice discharge from tidewater and lake-terminating glaciers, the mass balance of GOA glaciers during 1994–2013 has been dominated by mass losses from land terminating glaciers that are controlled primarily by climate variability [Larsen *et al.*, 2015]. The average length of streams connecting the glaciers to the ocean is approximately 10 km, resulting in rapid delivery of glacier-derived runoff and nutrients to estuaries and fjords, forming a strong link between the terrestrial hydrologic cycle and the nearshore environment [Hood *et al.*, 2015; O'Neil *et al.*, 2015].

3. Data and Methods

3.1. Water Balance and Hydrologic Partitioning

The water balance for the GOA watershed is given by

$$\frac{dS}{dt} = P - (ET + SU) - R - D \quad (1)$$

where S is the volume of water stored in the watershed, and the precipitation input P , evapotranspiration ET , snow sublimation SU , runoff R , and ice discharge D are all taken to be in rate form. In the GOA watershed, coastal FWD is the runoff R term, and glacier mass storage is a component of the S term. We assume D from tidewater glaciers to be a negligible contributor to FWD for reasons discussed below. We partition the hydrologic source water by separating the R term into three main constituent parts: meltwater from the snowpack base, direct rainfall onto snow-free surfaces, and meltwater from glacier ice surfaces once snowpack is removed. R can also be separated further into glacier and nonice land sources. All terms on the right hand side need to be determined to compare water storage changes with those from GRACE data.

The calculation of D is complex due to the difficulty in measuring and modeling calving fluxes from tidewater glaciers. Existing studies provide estimates of tidewater glacier frontal ablation, a term that includes iceberg calving (D) as well as the melt rate at the glacier terminus. Values range between 19 km³ w.eq. yr⁻¹ for the period 1980–1999 [Huss and Hock, 2015] and 15.1 km³ w.eq. yr⁻¹ for the period 1985–2013 [McNabb *et al.*, 2015], using model simulations and satellite observations, respectively. This is approximately 7–8% of annual average Alaska glacier ablation rates. Larsen *et al.* [2015] used airborne altimetry data to measure

1994–2013 Alaska glacier-wide mass changes due to climate and ice dynamics. They show that the combined tidewater glacier mass balance ($\sim -5 \text{ km}^3 \text{ w.eq. yr}^{-1}$) was less negative than land-terminating Alaska glaciers, likely due to a slowdown in their dynamic mass changes. Because these studies do not allow us to directly estimate the ice dynamics contribution to mass loss, we do not formally include D in our water balance calculations. Below we provide estimates of the possible impact of neglecting D on our cumulative mass balance calculations.

3.2. Model Description

SnowModel-HydroFlow is a suite of distributed, physically-based meteorological (MicroMet) [Liston and Elder, 2006a], energy-balance snow and ice melt (SnowModel) [Liston and Elder, 2006b], and linear-reservoir runoff routing (HydroFlow) [Liston and Mernild, 2012] models designed for climates and landscapes where snow and ice are present. We have added to this suite a simple soil water balance model (SoilBal) that simulates the pathways of precipitation and snowmelt in evapotranspiration, infiltration into soils, surface, and base flow runoff.

SnowModel and HydroFlow have previously been applied in large domain simulations to estimate trends in Pan-Arctic snow cover and depth using a 10 km grid size and 3 h time step [Liston and Hiemstra, 2011], Greenland ice sheet surface mass balance and freshwater discharge estimates using a 5 km grid size and daily time step [Mernild et al., 2011; Mernild and Liston, 2012], and northern hemisphere glacier and ice sheet surface mass balance using a 1 km grid size and 3 h time step [Mernild et al., 2014], among other studies. The following sections give a general description of each of the submodels we used, and how the input data (elevation, land cover, soil texture, and weather) were generated. Readers should refer to original publications for more detailed model descriptions. A list of primary model parameters, their default values, and key citations are given in Table A1 of the Appendix A. Section 3.4 provides a description of the model parameter optimization process.

3.2.1. MicroMet

MicroMet [Liston and Elder, 2006a] is a data assimilation and interpolation scheme that defines meteorological forcing conditions on the high-resolution grid of the DEM and land cover. We used MicroMet to interpolate air temperature, precipitation, humidity, wind speed, and wind direction from coarse-resolution reanalysis grid cell centers to a fine-scale model grid, based on known relationships between weather variables and topography. We also used MicroMet to generate solar and incoming longwave radiation estimates based on topographic slope, aspect, and cloud cover derived from relative humidity and temperature observations.

3.2.2. SnowModel

SnowModel [Liston and Elder, 2006b], is a spatially distributed snow evolution modeling system designed for application in landscapes and conditions where snow and ice occur. The model uses meteorological input from MicroMet to compute the full evolution of snow water equivalent (SWE) which includes: (1) accumulation from snow precipitation; (2) blowing-snow redistribution and sublimation; (3) snow-density and mass transfer evolution; and (4) snowpack ripening, refreezing, and melt water flow. SnowModel uses a surface energy balance approach to calculate the magnitude and timing of snow and ice melt. SnowModel was originally developed for glacier free landscapes, and was modified for glacier mass balance studies in Greenland to simulate glacier ice melt occurring after removal of the winter snowpack [Mernild et al., 2006; Mernild et al., 2014]. Here we used SnowModel to solve the surface energy balance and associated hydrologic fluxes on a subdaily time step, which enabled us to capture the diurnal fluctuations in snow and ice-melt, including hydrologically important rain-on-snow events. SnowModel does not include a glacier flow model, thus to avoid nonrealistic snow accumulation at high elevations during multiyear simulations we removed any residual snowpack at the end of the summer melt season each hydrological year. Therefore, the model does not conserve snowpack mass across years, and assumes that the residual on-glacier snowpack is converted to ice at the end of the melt season.

3.2.3. SnowModel Soil Moisture Submodel (SoilBal)

Hill et al. [2015] used remotely sensed data from MODIS Global Evapotranspiration Project (MOD16) to estimate an annual ET volume from the GOA basin of $135 \text{ km}^3 \text{ w.eq. yr}^{-1}$, roughly 17% of the annual runoff volume, highlighting the importance of the ET term in GOA water balance (equation (1)). Previous applications of SnowModel excluded calculation of ET because the simulations occurred during the winter season or in areas largely dominated by glaciers and ice sheets (Greenland) where ET fluxes are small.

The significance of the ET flux in the GOA basin motivated the following additions to the SnowModel model structure. First, we calculated potential evapotranspiration (PET) using the Priestley-Taylor equation [Priestley and Taylor, 1972], which uses modeled daily air temperature and top-of-canopy net radiation (R_n). We used a Priestley-Taylor coefficient (α) of 1.26, which is consistent with previous regional-scale applications [Federer et al., 1996; Shuttleworth, 2007]. The R_n calculation takes into account variations in surface albedo from different vegetation types. In the case where PET is negative (typically during winter when R_n is negative), PET was set to zero. Second, routines were added to solve a soil water balance [Flint et al., 2013] using SnowModel grid-cell runoff and PET as hydrologic input, and gridded soil water storage at field capacity and wilting point. The root zone water storage was calculated as the water content of the soil at a given condition (e.g., field capacity, wilting point) multiplied by the rooting zone depth, and was used to determine the soil moisture conditions in the soil water balance. For the different soils in the GOA, soil characteristics (percent sand, silt, clay) were used to calculate soil water content at field capacity (-0.03 MPa) and wilting point (-1.5 MPa) using the Rosetta model [Schaap et al., 2001]. Rooting zone depths for the different SnowModel vegetation classes in the GOA were estimated from Jackson et al. [1996], and ranged from 0.3 m (tundra) to 1.2 m (coniferous forest). These two processes together make up the submodel SoilBal. SoilBal produced daily grids of actual evapotranspiration (ET), surface, and base flow runoff. The resulting surplus runoff and base flow output were then used to drive the runoff simulations (section 3.2.4).

3.2.4. HydroFlow

The HydroFlow runoff routing model [Liston and Mernild, 2012; Mernild and Liston, 2012] simulates the routing of surface runoff produced from rainfall, snow, and ice melt across glaciers and land to downslope areas and basin outlets. Runoff is transported through the drainage network by a series of linear reservoirs, with each grid cell containing a slow and fast response reservoir. The slow response reservoir accounts for the time meltwater and rainfall takes to move through the snow/ice/soil matrices down to the fast response reservoir, which moves the water down network and simulates channel flow. A coupled system of equations solves for fast and slow-response flow and the final solution yields a discharge hydrograph for each grid cell. HydroFlow contains parameters that were adjusted to match simulated discharge hydrographs to available observations.

SnowModel daily output of cell runoff and SWE depth were used as input for the HydroFlow runs. Due to the computational constraints of the large number of cells in the domain and the number of individual watersheds for flow computations, HydroFlow was run in overlapping 2 year intervals, with the first year spinning up the flow network from rest. The second-year output files were then aggregated, resulting in a continuous time series of discharge at each grid cell. Summation of the hydrographs of all coastal cells provided the discharge of the entire GOA basin.

3.3. Model Forcing Data

3.3.1. Elevation and Land Cover

The model requires elevation, land cover, soil texture, and weather data. A hydrologically corrected (depression less) digital elevation model (DEM) was obtained from the U.S. Geological Survey (USGS) Hydro1K North America data set derived from the GTOPO30 data set. Vegetation classes for each grid cell were obtained from the 2006 National Land Cover Database (NLCD) [Fry et al., 2011]. The land cover grid was aligned with the DEM and reclassified to the vegetation classes defined in Liston and Elder [2006b]. Glacier ice cover (Figure 1c) was obtained from the Randolph Glacier Inventory (RGI; Version 3.2) [Pfeffer et al., 2014] and these data were used as the permanent ice land cover class in the SnowModel simulations. RGI shapefile polygons were converted to a 50 m grid, and then resampled to the 1 km model grid. Only 1 km grid cells with more than 50% glacier cover were considered glacier covered cells. The RGI coverage has a total glacier area of $72,392$ km 2 in the delineated GOA drainage, while the final SnowModel vegetation file has a gridded glacier area of $74,703$ km 2 , a 3.1% difference in area. To account for this difference, a scaling factor (CF = 0.969) was applied to the glacier-only model output. Soil texture data were obtained from the gridded Harmonized World Soil Data set (HWSD; Version 1.2) [Fischer et al., 2008], available at 1 km resolution.

3.3.2. Meteorological Forcing

The GOA region has a limited number of weather stations, with existing stations biased to low elevations. There are 102 active weather stations in the GOA operated by the National Climatic Data Center (NCDC). These NCDC stations are located mainly in the Cook Inlet and Southeast Panhandle areas, and 94% are

below 500 m a.s.l., whereas glaciers and mountains in the GOA exceed 5000 m a.s.l. In addition to this bias, complex topography limits the spatial representativeness of these station data [Royer, 1982; Wang *et al.*, 2004]. Therefore, we assembled time series of precipitation, 2 m air temperature and relative humidity, and 10 m wind speed and direction from a set of gridded reanalysis products. We used the National Centers for Environmental Prediction (NCEP) North American Regional Reanalysis (NARR) [Mesinger *et al.*, 2006], NASA Modern Era Retrospective Analysis for Research and Applications (MERRA) [Rienecker *et al.*, 2011], and NCEP Climate Forecast System Reanalysis (CFSR) [Saha *et al.*, 2010] products, which have (nominal) spatial resolutions of 32, 67, and 38 km, respectively, and temporal resolutions of 3, 3, and 6 h, respectively. For the NARR data set, rain-gauge observations in Canada were assimilated to aid precipitation analysis until December 2002; afterwards the hydrologic fields are entirely model derived [Lader *et al.*, 2016]. This produces an artificial shift in the annual total precipitation amount and seasonal pattern in the NARR data for areas of the GOA basin east of the 150°W meridian.

Initial testing revealed the NARR precipitation data had significantly lower precipitation values than the other two reanalysis products. We therefore attempted to improve the NARR product by bias-correcting it to high spatial resolution (2 km), low temporal resolution (monthly time series) weather grids of temperature and precipitation [Hill *et al.*, 2015] that were based on station data and Parameter-Elevation Regressions on Independent Slopes Model (PRISM) [Daly *et al.*, 1994] climatologies. The bias-correction procedure followed Abatzoglou [2011] except for that author's use of the PRISM monthly time series available for the conterminous United States [Daly *et al.*, 2008].

The bias-correction involved: (1) aggregating the NARR 3 hourly temperature and precipitation to a monthly time step and calculating mean temperature and summed precipitation at each NARR cell in the model domain from 1979 to 2009; (2) extracting monthly precipitation and temperature from the 2 km weather grid cell nearest to each NARR cell center over the same time period; and (3) adjusting estimates of 3 hourly temperature and precipitation on the 32 km NARR grid using equations (2) and (3). The bias-corrected temperature is given by:

$$T_R = T_N + T_G - \bar{T}_N \quad (2)$$

where T_N is the original NARR temperature, T_G is the monthly weather grid temperature, T_R is the bias corrected NARR data, and \bar{T}_N is the time-averaged NARR temperature for the given month and year. The bias-corrected precipitation is given by:

$$P_R = \left[\frac{P_N}{\sum P_N} \right] * P_G \quad (3)$$

where P_N is the original NARR data (3 hourly), P_G is the weather grid precipitation, and P_R is the bias-corrected NARR data. The summation in the denominator is carried out over all the days and over the eight time steps (3 hourly) per day for each month. Due to lack of fine-scale information, humidity, wind velocity, and wind direction were not modified.

3.4. Model Calibration

The distributed hydrologic model used in this study has a large number of parameters. Some of these parameters have well-constrained values that have been determined by physical principles and experimentation. Other model parameters depend strongly on the local glaciometeorological conditions and need to be determined using local data or by parameter optimization [Ragettli and Pellicciotti, 2012]. Table A1 in Appendix A shows a selection of the default model parameters for the SnowModel and HydroFlow submodels and supporting citations.

To inform the selection of model parameters, a phased approach was adopted. Four small-gaged catchments (Figure 2) were identified for initial simulations. The four local watersheds were selected based on the following criteria: (1) they possessed long-term glacier mass balance data sets required to evaluate and improve the model and input data sets; (2) they contained streamflow data from all of the primary stream types (rain, snowmelt, and glacially dominated) to ensure that the runoff model was being tested across different flow regimes; and (3) they sampled a range of different climatic and geographic zones, three being located in coastal locations, and one located further inland.

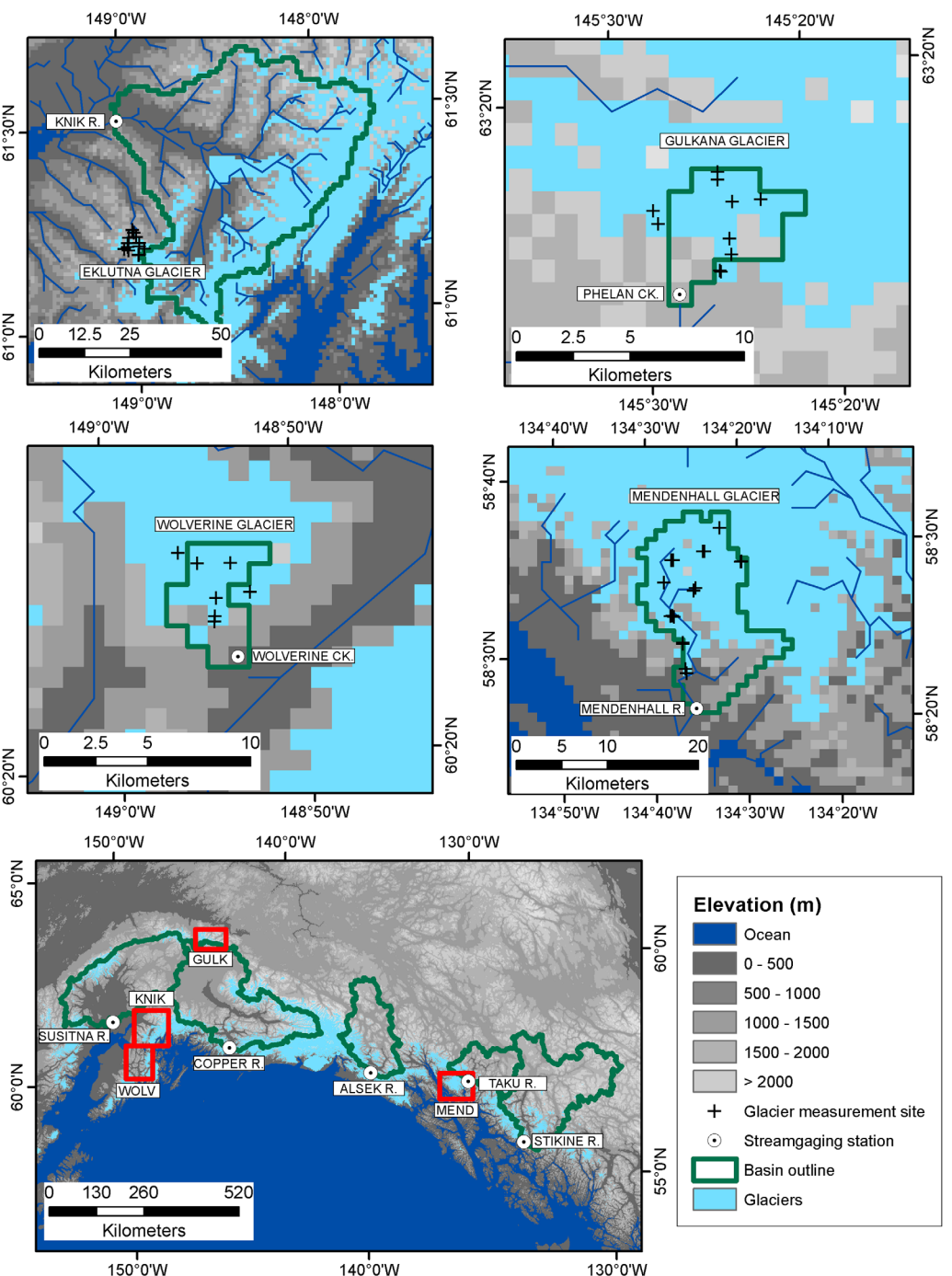


Figure 2. Map of the four local domains showing USGS stream gages and point balance locations used for model calibration. Dark blue lines indicate stream network and ocean cells, light blue cells are glacier covered. (bottom) The location of the local domains along the GOA coastline.

We first combined high-resolution PRISM climatologies with the DEM to construct monthly temperature-elevation and precipitation-elevation relationships for each watershed. Temperature lapse rates had a strong seasonal pattern, with lowest values ($2.5^{\circ}\text{C km}^{-1}$) in the winter months and highest values ($5.6^{\circ}\text{C km}^{-1}$) in the summer months. The largest difference in lapse rates between the local domains occurred during the winter months, due to the influence of temperature inversions in the two interior (Gulkana and Knik) drainages. The computed gradients in annual precipitation ranged from 0.7 m km^{-1} at Gulkana

Table 1. Calibration Stations for the Local Model Simulations (Locations Outlined in Red in Figure 2)^a

Region	Name	ID	Var.	Lat.	Lon.	Elev. m	Source	Dates
Knik	Knik River	15281000	Q	61.505	-149.031	9	USGS	1979–2013
	Eklutna Glacier	65	B	61.211	-148.978	1120–1550	Sass [2011]; Loso [2011]	2007–2012
Mend	Mendenhall River	15052500	Q	58.430	-134.537	18	USGS	1979–2013
	Mendenhall Glacier	98	B	58.497	-134.504	70–1580	Boyce <i>et al.</i> [2007]; University of Alaska Southeast [2015]	1998–2012
Wolv	Wolverine Creek	15236900	Q	60.371	-148.897	366	USGS	2000–2013
	Wolverine Glacier	270	B	60.412	-148.913	1470–1980	Van Beusekom <i>et al.</i> [2010]	1979–2013
Gulk	Phelan Creek	15478040	Q	63.241	-145.468	1125	USGS	1990–2013
	Gulkana Glacier	353	B	63.277	-145.415	1200–2010	Van Beusekom <i>et al.</i> [2010]	1979–2013

^aFor each model domain, observations of monthly stream discharge Q and seasonal glacier mass balance B were used to calibrate the model simulations. For B, the number of individual points is given in the ID column, along with the average latitude and longitude values and elevation range for the individual points.

Glacier to 2.5 m km⁻¹ at Mendenhall Glacier, similar to measured SWE gradients (1.15–4.0 m km⁻¹) for GOA glaciers reported in McGrath *et al.* [2015].

Next, to establish confidence in or adjust other model parameters for regional (GOA-wide) simulations of FWD, simulations of the four local watersheds were carried out. The goals of the local simulations were to (1) perform a sensitivity analysis to assess the influence of selected model parameters on modeled streamflow and mass balance results, and (2) optimize the values of the most influential parameters. This optimization was done independently for each weather-forcing product.

For each catchment, streamflow and glacier mass balance measurements were used for calibration (Table 1). Stream gages on Wolverine Creek, Phelan Creek, and Mendenhall River were located in the same watershed as the glacier being monitored. The Knik River stream gage was located in a large watershed adjacent to the monitored Eklutna Glacier, but we assume that glaciers in that watershed experience similar regional climate patterns due to close proximity (~20 km), and similar mean elevation and glacier aspect. These glacier mass balance observations were derived from biannual field measurements to determine winter, summer, and annual mass balances following conventional field mass balance techniques [Cogley *et al.*, 2011]. In the model simulations, glacier mass balance was determined as P – (R + SU).

While some of the model parameters are spatially variable (tied to land cover class), the majority are spatially constant. To determine which parameter value was best for the regional simulations, we evaluated the model runs based on the average performance across the four local domains. Specifically, model simulations of streamflow (Q) and mass balance (B) were evaluated against the available data using the root mean squared error (RMSE), Nash-Sutcliffe efficiency (NSE), and coefficient of determination (r^2) values. The goal was to minimize RMSE and maximize NSE and r^2 for both Q and B. After each model run, statistics were computed for Q and B in each local domain, and then a domain-averaged value was used to assess overall performance. Initial uncalibrated runs (default parameters in Table A1) yielded statistically significant ($p < 0.001$) domain-averaged NSE values of 0.72–0.87 for Q and r^2 values of 0.43–0.77 for B, where the range of values represents the results from the four weather products. These values then served as the benchmark for the parameter sensitivity analysis and parameter optimization model runs.

We initially considered six parameters for the calibration of the model. Similar to Ragletti and Pellicotti [2012], we selected model parameters important for the conditions in the mountainous, glacierized watersheds in Alaska, and grouped them according to their importance for (1) characterization of the late winter snowpack and rain/snow fraction, (2) simulation of surface melt at glacier and snow surfaces, and (3) transformation of surface meltwater into runoff (Table 2). Group 1 parameters were monthly varying precipitation adjustment factors (χ) and rain/snow threshold temperatures (T_{rain}/T_{snow}). The seasonal variability and magnitude of monthly χ values were informed from the PRISM precipitation data in the local domains. Sets of paired T_{rain} and T_{snow} values from Fuchs *et al.* [2001] were tested, using a linear interpolation between to determine the fraction of both snow and rain. Group 2 parameters were nonforested melting snow albedo ($\alpha_{s,melt-clearing}$) and glacier ice albedo (α_{ice}). Group 3 parameters were the fast and slow response times (k_f and k_s), where k_f represents the time scale of channel flow in streams and through glaciers, and k_s represents time scale of transport through snow and ice matrices, and soil.

Table 2. Optimized Calibration Parameters for Each Weather Product: High and Low Values of Monthly Precipitation Adjustment Factor (χ_{low} , χ_{high}), Snow/Rain Threshold Temperatures (T_{snow} , T_{rain}), Glacier Ice Albedo (α_{ice}), Melting Snow Albedo (α_{snow}), Slow Residence Time Scale (k_s), and Fast Residence Time Scale (k_f)^a

Data Set	Group 1		Group 2		Group 3	
	χ_{low} , χ_{high} (km^{-1})	T_{snow} , T_{rain} (°C)	α_{ice}	α_{snow}	k_s (h)	k_f (h)
MERRA	0.20, 0.35	0.0, 2.0	0.30	0.60	27.8	4.2
NARR	0.30, 0.53	0.0, 2.0	0.30	0.60	27.8	4.2
NARR-BC	0.20, 0.35	0.0, 2.0	0.40	0.60	27.8	4.2
CFSR	0.20, 0.35	0.0, 2.0	0.30	0.60	27.8	4.2

^aValues of k_s and k_f are shown for snow-free ice grid cells only.

We performed a sensitivity analysis where the six model parameters were perturbed individually from the default model value (within a range), and the resulting statistics were compared with those from the default run. The results (relative ranking) did not change depending upon the choice of performance metric (RMSE, NSE, r^2) so the definition of a composite metric was not needed. Our analysis showed that the model results were most sensitive to the values of four model parameters (χ , α_{ice} , k_f and k_s), and these were selected for optimization. T_{rain} and T_{snow} were set to 2°C and 0°C, respectively; $\alpha_{s,melt-clearing}$ was set to a value of 0.6 [Melloh et al., 2001]; albedo of fresh snow ($\alpha_{s,fresh}$) was given a value of 0.8.

3.5. GRACE Solution

We used data from the NASA/DLR Gravity Recovery and Climate Experiment (GRACE) satellites as an independent validation of our GOA runoff estimates. GRACE measures time variations in Earth gravity resulting from changes in atmospheric and oceanic mass, Earth and ocean tides, mantle dynamics and terrestrial hydrology including glaciers. We used the iterated v13 high-resolution mascon solution from the NASA Goddard Space Flight Center Space Geodesy Laboratory [Luthcke et al., 2013], updated to the June 2014 time period, and subsetted to the region of our model domain. This GRACE solution provides a measure of the time-averaged storage of mass within $1^\circ \times 1^\circ$ equal-area (approximately $12,390 \text{ km}^2$) mass concentration (mascon) grids, during approximately monthly sampling intervals [Arendt et al., 2013].

The GRACE mascon processing method attempts to isolate the glacier mass balance signal through forward modeling of glacial isostatic adjustments and changes in ocean tides, atmospheric mass, and terrestrial water storage, including snow accumulation and melting on nonglacier surfaces. Our solution utilizes the Global Land Data Assimilation System (GLDAS)/Noah land surface model 0.25°, 3 h data to represent terrestrial water storage variations [Rodell et al., 2004]. It is necessary to set these terrestrial water storage variations to zero over glacier surfaces because GLDAS predicts continuous accumulation of snowpack on model grid cells containing glaciers. This unrealistic behavior occurs because GLDAS does not account for glacier ice flow which redistributes accumulated snow over time. In addition, GLDAS has coarse resolution (0.25°) and is unable to resolve the highly distributed nature of glacier surface cover in Alaska. As a result, the magnitude of terrestrial water storage corrections applied within the GOA mascon domain is negligible, and the GOA mascon solution likely contains a significant component of both glacier and nonglacier snow and ice hydrology. In this paper, we used our modeling results to infer the extent to which existing GRACE mascon solutions for Alaska include both glacier and land surface hydrology signals, which is important for correct interpretation of GRACE data for hydrology and sea level studies.

3.6. Model Configuration

Using the modeling system described in section 3.2, land and ice hydrologic processes, including precipitation, snow accumulation, sublimation, evapotranspiration, runoff, glacier surface mass balance, and stream discharge were simulated for the 35 year period September 1979 through August 2014. The model domain covered a $1810 \text{ km} \times 900 \text{ km}$ grid centered over the GOA drainage and used a subdaily time step (3 h for MERRA, NARR, and NARR-BC; 6 h for CFSR) at a 1 km spatial resolution. Model results were aggregated from subdaily to daily for the purposes of output. The gridded results provided information at individual grid cells of interest (e.g., at a stream gage) and were also aggregated to a variety of geographic regions and time steps of interest. For example, we used equation (1) to calculate a time series of the storage in the entire GOA domain. Additionally, in order to calculate the annual mass accumulation (snow accumulation), ablation (melting of snow and ice, sublimation), and storage change (snowpack and glacier ice) for the drainage

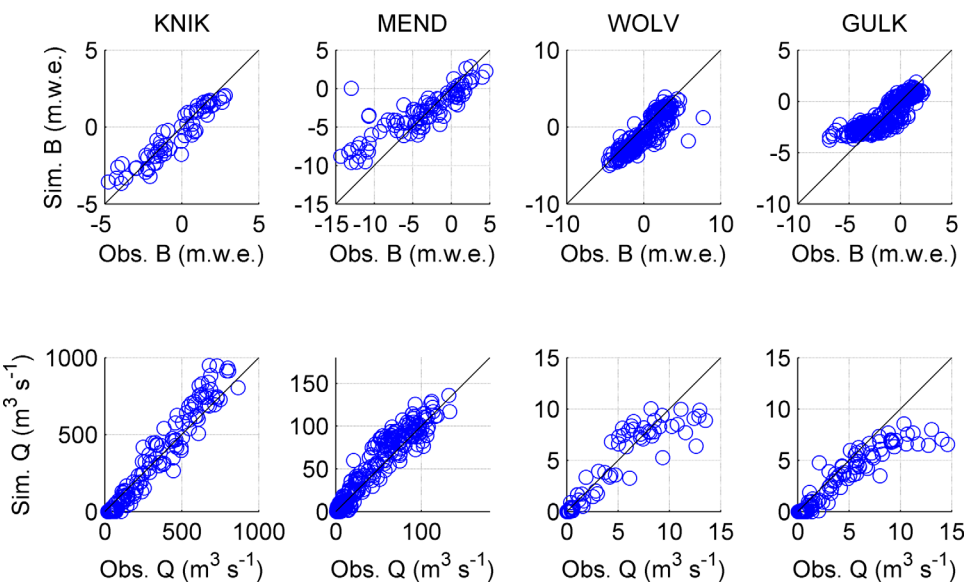


Figure 3. (top: Sim. B) Sample scatterplots of simulated seasonal glacier mass balance in meters of water equivalent (m.w.e) and (bottom: Sim. Q) monthly discharge in cubic meters per second compared with observations (Obs.) from the Knik (KNIK), Mendenhall (MEND), Wolverine (WOLV), and Gulkana (GULK) domains. Results are shown for simulations driven with MERRA forcing using the best fit parameters.

basin and glacier surfaces, we used standard glaciological mass balance methods based on the annual maxima and minima of the water storage time series [Østrem and Brugman, 1991].

4. Results

4.1. Local Domain Calibration

A sample comparison of simulated and observed streamflow and glacier mass balance at the four local domains using the MERRA forcing is shown in Figure 3. The final calibrated model parameters for each weather product are shown in Table 2.

We used a spatially averaged statistical value across the four local domains as criteria for determining the ranking (Table 3) of the weather forcing products. For streamflow, we used the NSE value and for glacier mass balance, we used the r^2 value. These selections were made since those are the most commonly used performance metrics in the respective fields. For streamflow, ranking from best to worst was CFSR, MERRA, NARR, and NARR-BC with domain-averaged NSE values of 0.89, 0.88, 0.82, and 0.74, respectively. For glacier mass balance, the ranking was MERRA, CFSR, NARR, and NARR-BC with domain-average significant ($p < 0.001$) r^2 values of 0.78, 0.68, 0.62, and 0.43, respectively. MERRA and CFSR showed very comparable agreement with observed streamflow and MERRA had the best overall agreement with glacier mass balance. Based on these criteria, we determined that the MERRA data set had the best overall performance in the local domain simulations, closely followed by CFSR.

In addition to comparing model output to observations of Q and B, we also evaluated SnowModel's snow simulation performance for the regional simulations by comparing observed and modeled 1980–2009 average 1 April SWE (proxy for peak snow accumulation) between 23 SnoTel sites in the GOA and corresponding 1 km model pixels. Modeled SWE from both MERRA and CFSR runs suggest some positive simulation bias but acceptable performance overall. MERRA had a smaller model bias and standard deviation (0.04 and 0.16 m w.eq.) than CFSR (0.26 and 0.25 m w.eq.) for the regional SWE simulations. Discrepancies between individual observed and simulated SWE values can be attributed to a combination of model error as well as to the effects of scale mismatch and possible lack of representativeness between SnoTel snow pillow sites and model pixels [Schnorbus et al., 2014].

4.2. GOA Regional Water Balance

Regional simulations of the water balance fluxes from equation (1) (P, R, SU, ET) as well as SWE depth and Q were carried out using the four climate products described above. We analyzed SnowModel output for all

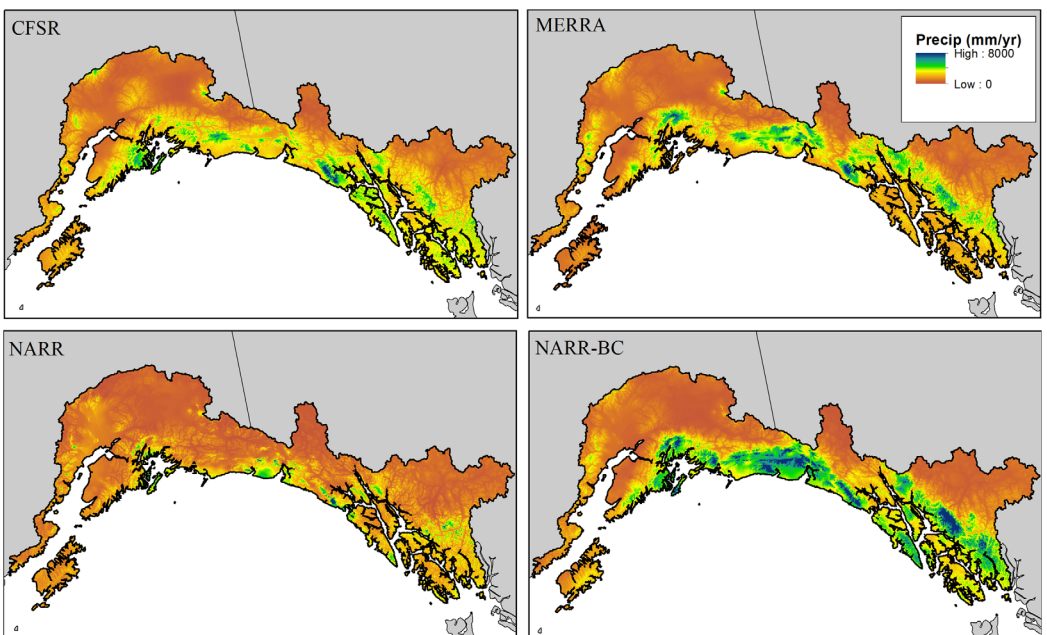
Table 3. Root Mean Squared Error (RMSE), Coefficient of Determination (r^2), and Nash-Sutcliffe Efficiency (NSE) Computed for Local Domain Simulations Using the Highest Performing Parameter Set for Each Weather Product in Each Region^a

Region	Data Set	Glacier Mass Balance, B			Stream Discharge, Q		
		RMSE (m)	r^2	NSE	RMSE ($m^3 s^{-1}$)	r^2	NSE
KNIK	MERRA	0.66	0.89	0.88	72.48	0.96	0.91
	NARR	0.86	0.81	0.80	80.06	0.95	0.89
	NARR-BC	2.29	0.01	-0.16	176.60	0.74	0.47
	CFSR	1.10	0.69	0.68	72.91	0.96	0.91
MEND	MERRA	2.77	0.80	0.67	10.93	0.95	0.91
	NARR	3.29	0.72	0.53	15.78	0.90	0.81
	NARR-BC	4.05	0.61	0.33	14.50	0.92	0.84
	CFSR	3.80	0.63	0.37	10.95	0.95	0.91
WOLV	MERRA	1.44	0.64	0.64	1.41	0.92	0.88
	NARR	2.03	0.29	0.28	2.15	0.82	0.72
	NARR-BC	2.03	0.31	0.30	1.66	0.90	0.83
	CFSR	1.44	0.64	0.64	1.42	0.92	0.88
GULK	MERRA	1.00	0.81	0.77	1.42	0.87	0.82
	NARR	1.31	0.67	0.60	1.34	0.88	0.84
	NARR-BC	0.99	0.80	0.76	1.41	0.87	0.82
	CFSR	1.09	0.77	0.72	1.32	0.89	0.85
MEAN	MERRA^b	1.47	0.78	0.74	21.56	0.93	0.88
	NARR	1.87	0.62	0.55	24.83	0.89	0.82
	NARR-BC	2.34	0.43	0.31	48.54	0.85	0.74
	CFSR	1.85	0.68	0.60	21.65	0.93	0.89

^aAll r^2 values were statistically significant ($p < 0.001$).^bBold values denote the mean statistic computed from the four regions.

the land and glacier surfaces in the GOA watershed shown in Figure 1 (land and ice), and for just cells entirely occupied by glacier ice (ice-only).

Mean annual GOA precipitation is 820, 760, 560, and 930 $\text{km}^3 \text{w.eq. yr}^{-1}$ for CFSR, MERRA, NARR, and NARR-BC respectively. Despite this large range in the total precipitation volume, each weather product produces approximately a 1:1 rain-snow fraction. Downscaled mean annual precipitation from the four weather data sets over the GOA basin show that the highest precipitation rates occur in the Chugach, St. Elias, and Coast

**Figure 4.** Maps of modeled mean annual precipitation (in mm yr^{-1}) from MicroMet for the four weather data sets, averaged over the period 1980–2009.

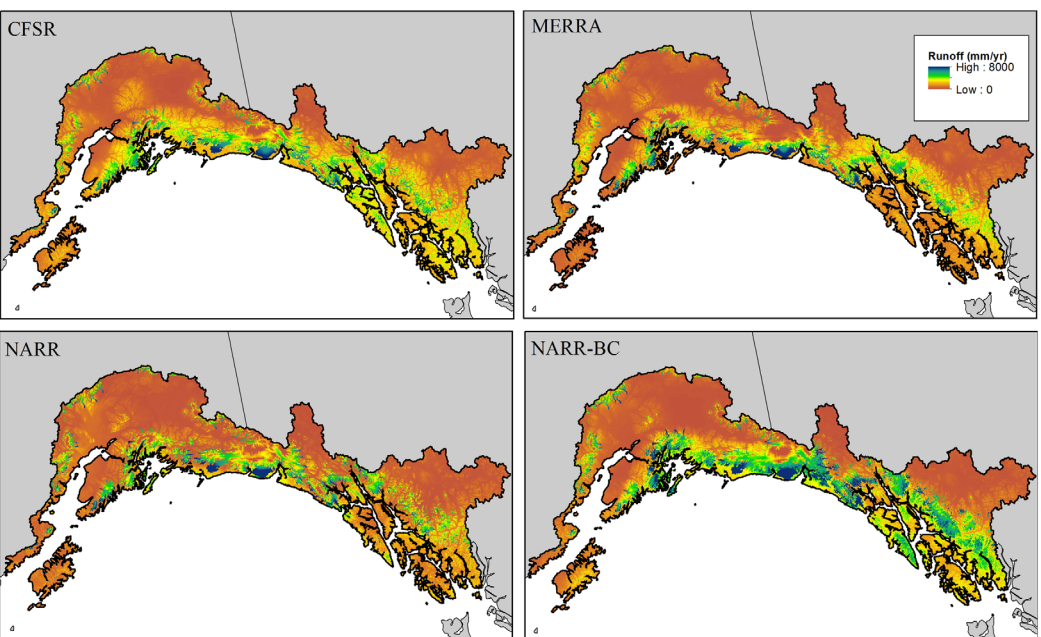


Figure 5. Maps of modeled mean annual runoff depth (in mm yr^{-1}) from SnowModel-SoilBal for the four weather data sets, averaged over the period 1980–2009.

Mountains, at rates $>8 \text{ m w.eq. yr}^{-1}$ (Figure 4). The NARR data set produces noticeably lower mountain precipitation than the other three data sets.

Mean annual runoff from the GOA drainage basin for CFSR, MERRA, NARR, and NARR-BC is 760, 630, 620, and $870 \text{ km}^3 \text{ w.eq. yr}^{-1}$, respectively. The majority of the runoff (Figure 5) is generated in the mountains, areas which receive large amounts of snow and rain. The highest runoff rates in the GOA basin occur at the low elevation regions of large coastal glaciers, at rates $>8 \text{ m w.eq. yr}^{-1}$. Mean annual runoff from GOA glacier surfaces for CFSR, MERRA, NARR, and NARR-BC is 290, 260, 310, and $400 \text{ km}^3 \text{ w.eq. yr}^{-1}$, respectively. The fraction of glacier runoff to total runoff (using annual average values over the entire simulation period) ranged from 38% for CFSR to 50% for NARR. The larger glacier runoff fraction from simulations forced with NARR data results from lower mountain snow accumulation and warmer temperatures than the other reanalysis products.

Mean annual combined ET and snow sublimation from the GOA drainage basin for CFSR, MERRA, NARR, and NARR-BC is 115, 123, 114, and $125 \text{ km}^3 \text{ w.eq. yr}^{-1}$, respectively. These estimates are 10–15% less than the mean MODIS ET value of $135 \text{ km}^3 \text{ w.eq. yr}^{-1}$ reported in Hill et al. [2015]. The highest ET rates occur in southeast Alaska and in the low elevations of the inland river basins.

The phase of precipitation input is a function of air temperature, and thus follows a strong seasonal cycle (Figure 6). Snowfall dominates the precipitation input during the winter months (November–March), while rainfall dominates during the summer season (June–September). During transition seasons (April–May, October), precipitation is more evenly mixed between rain and snow across the region. Hydrologic outputs also follow a strong seasonal cycle with peaks in both runoff and ET occurring during the months of June and July, when temperature and radiation forcing are at maximum values and available snowpack and glacier ice are melting. Runoff during the winter months is due to rainfall and snowmelt events that occur at low elevation coastal locations.

We partition the runoff from glaciers and the surrounding land into snow melt, glacier ice melt, and direct rainfall runoff and compute statistics (mean, standard deviation, and linear trend) of the annual time series for the full simulation period (Table 4). Although each climate product produces a positive trend in modeled total runoff, ranging from 1 to $2 \text{ km}^3 \text{ w.eq. yr}^{-1}$, the only trends significant at the 95% confidence limit are from NARR for total runoff, direct rainfall, and snowmelt components. The removal of rain-gage observations from the NARR precipitation analysis in January 2003 resulted in a step-change increase in total precipitation input of up to twofold for GOA regions east of 150°W , and generated increased runoff volumes from rainfall and snowmelt for the period 2003–2014 compared to 1980–2002. The positive trend for modeled glacier runoff is

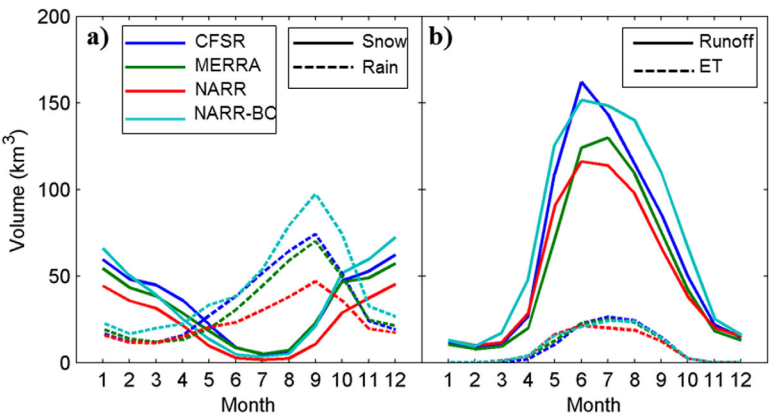


Figure 6. Mean monthly volumes of water balance components for the entire GOA basin. (a) Precipitation input from weather products and MicroMet partitioned into snow (solid line) and rain (dashed line). (b) Hydrologic outputs from SnowModel-SoilBal (right plots) partitioned into runoff (solid line) and ET (dashed line).

not statistically significant ($p > 0.05$) for any of the weather products. CFSR, MERRA, and NARR-BC have similar partitioning of the runoff, with 59–64% from snow melt, 17–20% from glacier ice melt, and 18–22% from direct rainfall. NARR has a slightly different partitioning with 49%, 33%, and 18% coming from snow melt, glacier ice melt, and rainfall, respectively. Snow melt dominates the runoff from April to June, glacier ice melt dominates from July to September, and rainfall runoff dominates from August to October (Figure 7). CFSR has a maximum runoff volume in June which is dominated by snowmelt. The other three data sets have maximum runoff occurring in July, from a more balanced mixture of snowmelt, ice melt, and rainfall.

Differences in the climate forcing data sets generate large differences in predicted water balances over the January 2003 to July 2014 simulation period (Figure 8), which is the period that overlaps with available GRACE data. The annual GOA water balance for hydrological years 2004–2013 was computed for GRACE and each model run (Table 5). The MERRA simulations produce a small gain in stored water ($6.8 \text{ km}^3 \text{ w.eq. yr}^{-1}$) while NARR generates a loss ($-158.2 \text{ km}^3 \text{ w.eq. yr}^{-1}$) during the simulation period. Trends in both NARR-BC ($-48.5 \text{ km}^3 \text{ w.eq. yr}^{-1}$) and CFSR ($-48.7 \text{ km}^3 \text{ w.eq. yr}^{-1}$) more closely match the GRACE trend of $-60.1 \text{ km}^3 \text{ w.eq. yr}^{-1}$. There are only small differences between trends for ice-only versus land + ice simulations. For the ice-only cells, all simulations produce losses in stored water (equivalent to glacier volume loss); the mean annual water balance was -58.9 , -12.7 , -158.6 , and $-71.5 \text{ km}^3 \text{ w.eq. yr}^{-1}$ for CFSR, MERRA, NARR, and NARR-BC, respectively.

All simulations generate seasonal patterns in the land + ice hydrology that have larger amplitudes than the ice signal alone. In all simulations, the ice-only average seasonal amplitudes (166, 170, 166, and 216 km^3

Table 4. Annual Time Series Statistics for Runoff Components From the Different Weather Products for the GOA Drainage Basin^a

Data Set	Statistic	Total Runoff	Glacier Runoff	Ice Melt	Snow Melt	Direct Rainfall
CFSR	Mean ($\text{km}^3 \text{ yr}^{-1}$)	758	286	127	483	148
	St. Dev. ($\text{km}^3 \text{ yr}^{-1}$)	58	32	23	44	27
	Trend ($\text{km}^3 \text{ yr}^{-1} \text{ yr}^{-1}$)	1.44	0.12	-0.18	1.12	0.50
MERRA	Mean ($\text{km}^3 \text{ yr}^{-1}$)	100	38	17	64	20
	St. Dev. ($\text{km}^3 \text{ yr}^{-1}$)	630	264	123	392	116
	Trend ($\text{km}^3 \text{ yr}^{-1} \text{ yr}^{-1}$)	1.48	0.72	0.20	0.71	0.57
NARR	Mean ($\text{km}^3 \text{ yr}^{-1}$)	100	42	19	62	18
	St. Dev. ($\text{km}^3 \text{ yr}^{-1}$)	621	307	206	303	111
	Trend ($\text{km}^3 \text{ yr}^{-1} \text{ yr}^{-1}$)	54	28	25	33	26
NARR-BC	Mean ($\text{km}^3 \text{ yr}^{-1}$)	2.02	0.07	-0.45	1.08	1.39
	St. Dev. ($\text{km}^3 \text{ yr}^{-1}$)	100	50	33	49	18
	Trend ($\text{km}^3 \text{ yr}^{-1} \text{ yr}^{-1}$)	869	395	173	506	190
	Mean ($\text{km}^3 \text{ yr}^{-1}$)	74	36	24	59	34
	St. Dev. ($\text{km}^3 \text{ yr}^{-1}$)	1.18	0.12	0.09	1.16	-0.07
	% of total runoff	100	45	20	58	22

^aTrend values in bold indicate significant trends ($p < 0.05$).

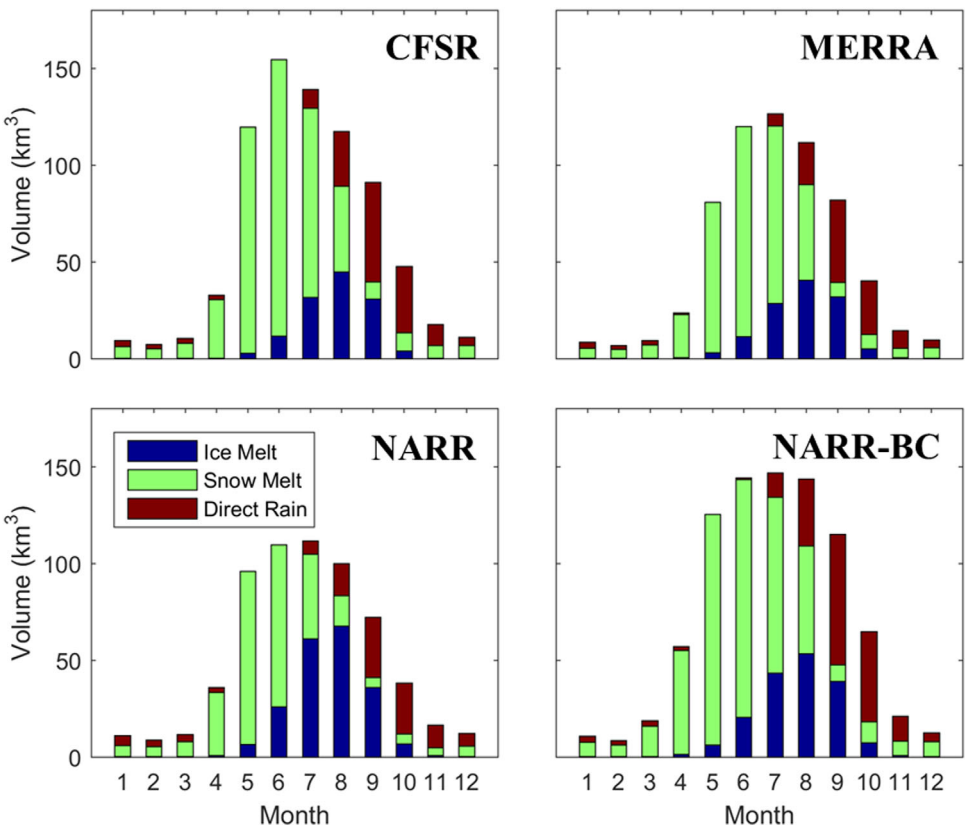


Figure 7. Stacked plots of mean monthly runoff volume from the GOA basin partitioned into following components: glacier ice melt, snow melt, and direct rainfall runoff. Mean monthly volumes were determined from daily model output over the period 1980–2014 for CFSR, MERRA and NARR, and 1980–2009 for NARR-BC.

w.eq. yr^{-1} for CFSR, MERRA, and NARR-BC, respectively) were less than the average seasonal amplitude of $325 \text{ km}^3 \text{ w.eq. yr}^{-1}$ measured by GRACE. All simulations produced ice + land average seasonal amplitudes ($409, 365, 333$, and $461 \text{ km}^3 \text{ w.eq. yr}^{-1}$ for CFSR, MERRA, NARR, and NARR-BC, respectively) that more closely matched GRACE. Both the trend and amplitude of the CFSR-forced land + ice model run most closely matched the GRACE observations.

Seasonal accumulation and melt for the GOA watershed for each year overlapping GRACE data (2004–2013), and averaged values over the period, are shown in Figure 9. From 2004–2013, the GRACE data had an annual accumulation of $295 \text{ km}^3 \text{ w.eq. yr}^{-1}$ and ablation of $355 \text{ km}^3 \text{ w.eq. yr}^{-1}$, most similar to the MERRA annual accumulation of $367 \text{ km}^3 \text{ w.eq. yr}^{-1}$ and melt of $361 \text{ km}^3 \text{ w.eq. yr}^{-1}$ over the entire (land + ice) GOA watershed. MERRA annual accumulation and ablation from GOA glacier cells account for 57% and 51% of the total watershed values, respectively.

4.3. GOA Freshwater Discharge

Mean monthly discharge from all GOA coastal cells is shown in Figure 10. The aggregated discharge for all four model runs has an annual maximum in July ranging from $46,000$ to $60,000 \text{ m}^3 \text{ s}^{-1}$ and an annual minimum in February ranging from $3,400$ to $4,300 \text{ m}^3 \text{ s}^{-1}$. The mean annual discharge ranges from $20,000$ to $27,600 \text{ m}^3 \text{ s}^{-1}$. The mean annual ice-only water balance values listed above were used to estimate the contribution of long-term losses in stored water on glaciers (GVL) to FWD from CFSR, MERRA, NARR, and NARR-BC to be 8%, 2%, 28%, and 9%, respectively. Previous estimates of GVL contribution to FWD were 7% [Hill *et al.*, 2015] and 10% [Neal *et al.*, 2010] made using independent estimates of GVL from GRACE and regional altimetry. This is the first study to directly model the linkages between FWD and GVL in this region.

Individual watersheds draining to the coastline, each with a mean annual total runoff and glacier runoff volume from CFSR, were ordered from smallest (2 km^2) to largest ($64,696 \text{ km}^2$), and the cumulative area and

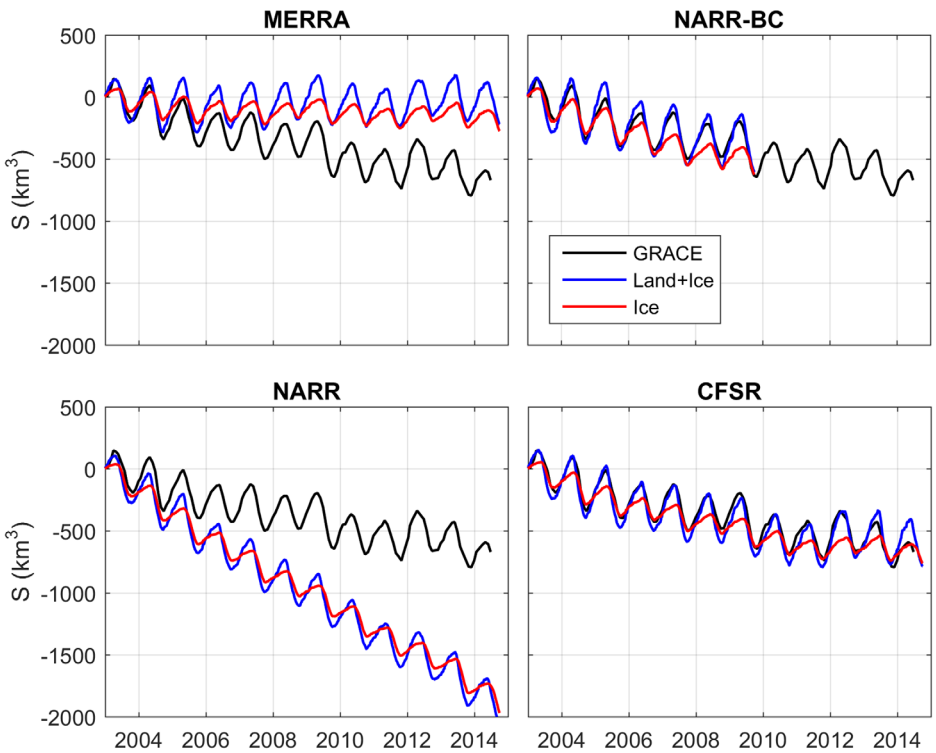


Figure 8. Cumulative water storage (S) determined from the GRACE mascon solutions and SnowModel simulations from January 2003 to September 2014.

runoff volume were calculated (Figure 11). Coastal watersheds with areas less than $1,000 \text{ km}^2$ ($n = 14,098$), indicated by the red and cyan polygons, make up 34% of the total area and contribute 48% of the total runoff and 40% of the glacier runoff volume. Coastal watersheds with areas between $1,000$ and $10,000 \text{ km}^2$ ($n = 24$), indicated by the green polygons, make up 15% of the total area and contribute 19% of the total runoff and 29% of the glacier runoff volume. The large inland watersheds with areas greater than $10,000 \text{ km}^2$ ($n = 5$), indicated by the blue polygons, make up the remaining 51% of the area, 33% of total runoff, and 31% of the glacier runoff volume. These results show the very large fraction of distributed (non-point) runoff typical of coastal landscapes occupied by glaciers.

5. Discussion

We find that MERRA and CFSR both perform well in terms of glacier mass balance and streamflow in the small, glacierized local watersheds. However, over the entire watershed, MERRA greatly underestimates the long-term changes in GOA water storage predicted by GRACE, while CFSR compares very favorably both

Table 5. Annual Water Balance for GOA Land + Ice Between 2004 and 2013 in Units of Volume ($\text{km}^3 \text{ yr}^{-1}$), Calculated as the Difference Between Successive Annual Mass Minima

Balance Year	GRACE ($\text{km}^3 \text{ yr}^{-1}$)	CFSR ($\text{km}^3 \text{ yr}^{-1}$)	MERRA ($\text{km}^3 \text{ yr}^{-1}$)	NARR ($\text{km}^3 \text{ yr}^{-1}$)	NARR-BC ($\text{km}^3 \text{ yr}^{-1}$)
2004	-149.0	-138.8	-60.5	-199.1	-80.8
2005	-55.5	-84.4	-6.8	-192.8	-55.4
2006	-28.0	-20.7	42.4	-127.9	-43.6
2007	-73.6	-85.3	-7.2	-173.4	-68.9
2008	16.5	-4.9	84.2	-107.6	-4.6
2009	-161.3	-104.7	-36.9	-164.0	-37.8
2010	-45.4	-59.0	-0.8	-164.0	
2011	-50.8	-19.2	-0.7	-151.0	
2012	78.5	80.6	92.4	-98.7	
2013	-132.3	-50.1	-38.1	-203.3	
Mean	-60.1	-48.7	6.8	-158.2	-48.5

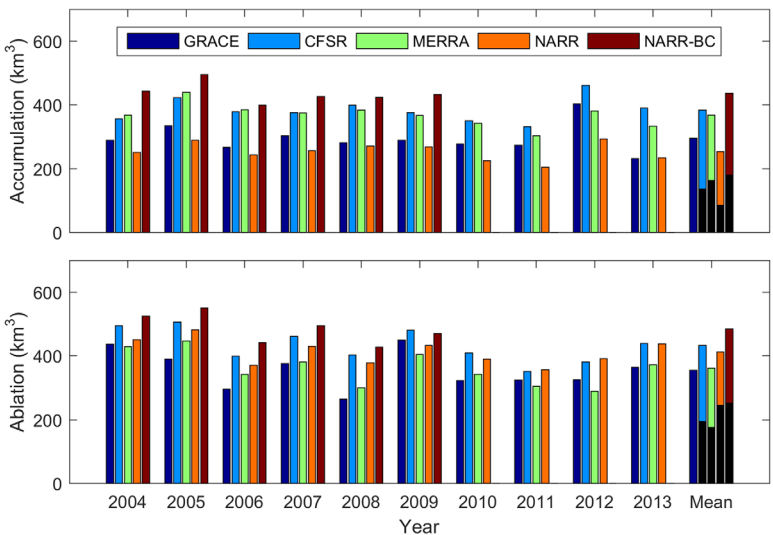


Figure 9. (top) Seasonal accumulation and (bottom) ablation of stored water from snowpack (land + ice surfaces) and glacier ice in the GOA watershed for balance years 2004–2013. Black bars in “Mean” column indicate the amount of annual accumulation and ablation occurring on glacier-only cells, averaged over the 10 year period.

with the trend and amplitude of the GRACE time series. As an additional regional validation, we calculated the 1994–2013 average GVL subsampled from the regional airborne altimetry data set of *Larsen et al.* [2015], yielding $-64 \pm 10 \text{ km}^3 \text{ w.eq. yr}^{-1}$. This is similar to the CFSR-predicted GVL trend of $-60 \text{ km}^3 \text{ w.eq. yr}^{-1}$ from 1980 to 2014. The MERRA data set predicts a GVL too low ($-12 \text{ km}^3 \text{ w.eq. yr}^{-1}$) because of a high precipitation value, and NARR predicts a GVL too high ($-171 \text{ km}^3 \text{ w.eq. yr}^{-1}$) because of low precipitation input. We therefore conclude that CFSR is the most suitable forcing data set for simulating the water balance of the GOA region, yielding a best estimate for runoff of $760 \text{ km}^3 \text{ w.eq. yr}^{-1}$, 8% of which is due to GVL. Our results highlight the need to verify model results using multiple data sources (ground observations, remote sensing) which sample the full water balance, and to examine the quality of input meteorological forcing derived from different weather products.

The mean annual FWD value of $760 \text{ km}^3 \text{ w.eq. yr}^{-1}$ ($1.80 \text{ m w.eq. yr}^{-1}$), is bracketed by the estimates of 725, 728, 850, and 870 obtained by *Royer* [1982], *Wang et al.* [2004], *Hill et al.* [2015], and *Neal et al.* [2010].

The mean annual glacier runoff value of $286 \text{ km}^3 \text{ w.eq. yr}^{-1}$, or $3.82 \text{ m w.eq. yr}^{-1}$, is larger than the mean annual glacier runoff value of $3.31 \text{ m w.eq. yr}^{-1}$ reported for Alaskan glaciers by *Mernild et al.* [2014] for the period 1979–2009 using SnowModel driven with MERRA. It is important to note that in that study the precipitation input was reduced by 30% to match observed mass balance, which likely decreased the glacier runoff depth. The values found by the NARR and MERRA simulations fall well below these previous studies, and the NARR-BC value of $870 \text{ km}^3 \text{ w.eq. yr}^{-1}$ falls on the upper bound. Our GVL estimate (8% of the total discharge) is slightly smaller than 10% reported by *Neal et al.* [2010].

Previous studies have assumed that the GRACE solution presented here represents the cumulative glacier mass balance

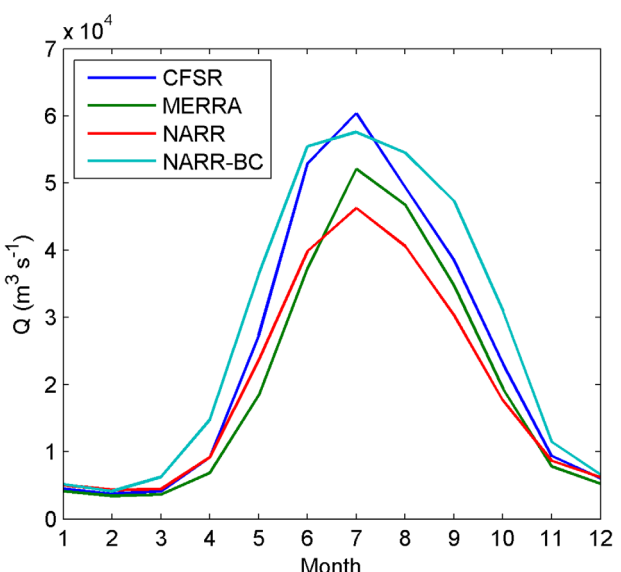


Figure 10. Climatology of mean monthly discharge along the entire GOA coastline.

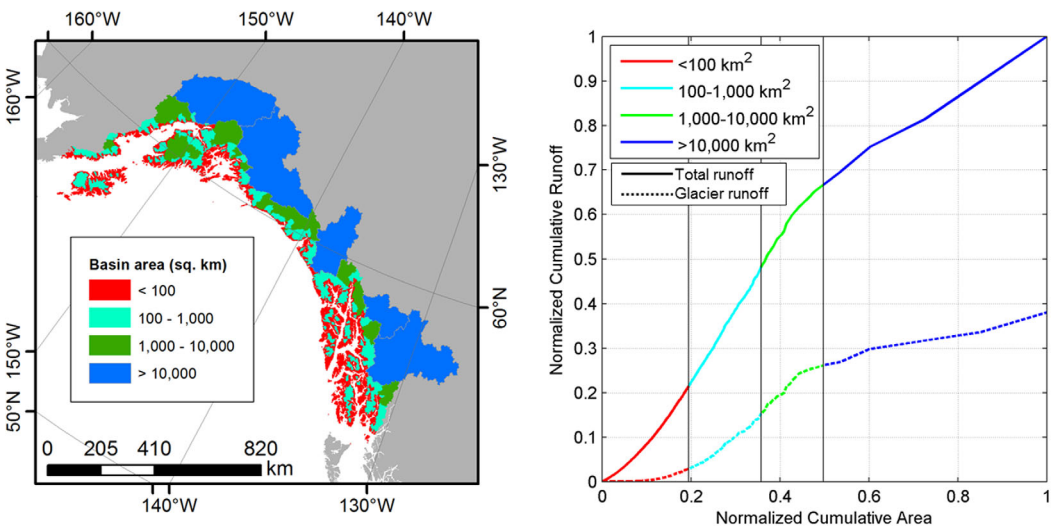


Figure 11. Map of the individual coastal watersheds in the GOA, color-coded by area. Plot shows the distribution of runoff volume by watershed size, ordered from smallest to largest watersheds. Lines vary in color based on the size of the watershed contributing runoff. The x axis is cumulative watershed area, normalized by the total GOA area ($420,300 \text{ km}^2$), and the y axis is the cumulative runoff volume, normalized by the total GOA runoff volume from the CFSR run (760 km^3).

of GOA glaciers [Arendt *et al.*, 2013; Luthcke *et al.*, 2013]. Those studies assumed the mass signals associated with terrestrial water storage variations on nonglacier surfaces had been adequately removed using independent data sets. Our CFSR model results that include land + ice surfaces agree much better with GRACE data than simulations for ice surfaces alone. Our findings are similar to those of Lenaerts *et al.* [2013] who found better agreement between GRACE and modeled hydrology that included both ice and tundra surfaces in the Canadian High Arctic. Our results highlight the complexity of partitioning hydrological signals using gravimetric data, and the utility of regional runoff models for refining our understanding of the GRACE time series. We find that glacier runoff (the sum of rainfall, snow, and ice melt occurring on glacier surfaces) accounts for only 38% of the average annual FWD signal, suggesting the magnitude of seasonal glacier mass balances from previous GRACE assessments are likely overestimates, and that a significant portion of that mass is due to runoff from nonglacier surfaces. We note that previous GVL estimates determined from GRACE mass trends remain valid, due to the disappearance of seasonal snowpacks from land surfaces each hydrological year.

Seasonal snowmelt is the dominant runoff term in our CFSR simulations. Therefore the accuracy of our model estimate depends strongly on the precipitation forcing fields, which in this study vary by $\sim 400 \text{ km}^3 \text{ w.eq. yr}^{-1}$ between data sets due to limited ground data and the difficulties in measuring and parameterizing precipitation processes. Improvements to our simulations can be achieved through expansion of field, airborne, and satellite missions dedicated to precipitation and snow cover measurements.

Our simulations do not account for hydrologic processes of lake storage, permafrost (ground ice), and groundwater storage. Watersheds in our study area have limited surface and subsurface water storage and these terms are likely small relative to the large seasonal fluctuations in snowpack and glacier volume [Kane and Yang, 2004]. We calibrated our model parameters that determine meteorological distribution, snow/ice melt, and runoff-routing in relatively small, steep, glaciated watersheds typical of the coastal watersheds along the GOA coastline. The model parameters were optimized for the most dynamic watersheds because we aimed to recover the largest proportion of the hydrologic signal. Therefore, we caution against using a subset of our results especially in regions that differ greatly from the calibration watersheds. In general, our results are optimized for the regional picture and more work is needed to ensure specific watersheds are well calibrated.

Our simulations also do not account for the adjustment of glacier geometry that occurs as ice flows to redistribute mass in response to a climate forcing. We use a fixed glacier area that represents conditions during 2006–2011, toward the end of our simulations period, because these are the highest quality glacier outlines available [Pfeffer *et al.*, 2014], and no data exist for the 1980s period. Given the widespread retreat of glaciers

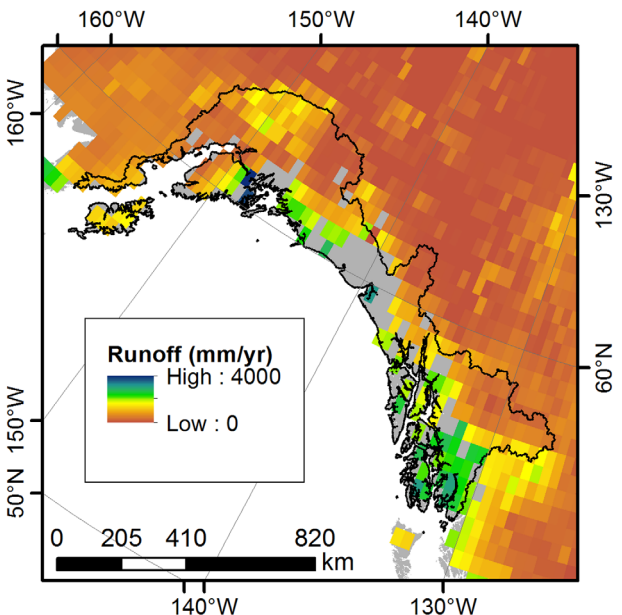


Figure 12. Gridded mean annual runoff from the Global Composite Runoff Fields [Fekete et al., 2002] database. Spatial resolution is 0.5° and gray cells report no data. The GOA watershed is indicated by the black line.

the Central Alaska Range, followed by the Western and Eastern Chugach Mountains. The highest relative debris cover occurs at the low elevations. We would expect regions with thin debris cover to have enhanced ice melt, while regions with thick debris cover reduced melt rates, compared with a clean ice surface [Reid and Brock, 2010]. Without knowledge of debris thickness, it is difficult to assess the implications of debris cover on the regional glacier mass balance.

Neglecting D from our water balance calculations likely has a minimal impact on our overall results. As noted above, Larsen et al. [2015] found that tidewater glaciers appear to be contributing less to Alaska glacier mass losses than any time since the end of the Little Ice Age, likely due to their retracted position and lack of extensive ice area at low elevations. If all GVL from Alaska's tidewater glaciers resulted from calving losses alone, then $5 \text{ km}^3 \text{ yr}^{-1}$ would be a minimum estimate for D . Considering frontal ablation, the values of $15\text{--}19 \text{ km}^3 \text{ w.eq. yr}^{-1}$ estimated in previous studies represent maximum values, because they include D as well as the surface mass balance of the terminus. To test the sensitivity of our results to the inclusion of D , we select the median value between the altimetry and frontal ablation estimates ($7 \text{ km}^3 \text{ w.eq. yr}^{-1}$) and apply this to our cumulative mass balance estimates. We find that including D changes the mean annual ice-only water balance for CFSR, MERRA, NARR, and NARR-BC to -67 , -19 , -178 , and $-83 \text{ km}^3 \text{ w.eq. yr}^{-1}$, respectively, an increase of 12%, 59%, 4%, and 9%, respectively, from the uncorrected values. With the exception of the MERRA data set, this correction is small relative to other error terms. These corrected values

are likely the lower limit (most negative) because this correction assumes all GVL from tidewater glaciers is due to iceberg calving.

The advances that this study makes in predicting coastal freshwater discharge are highly relevant to local and regional oceanographic processes in the Gulf of Alaska and

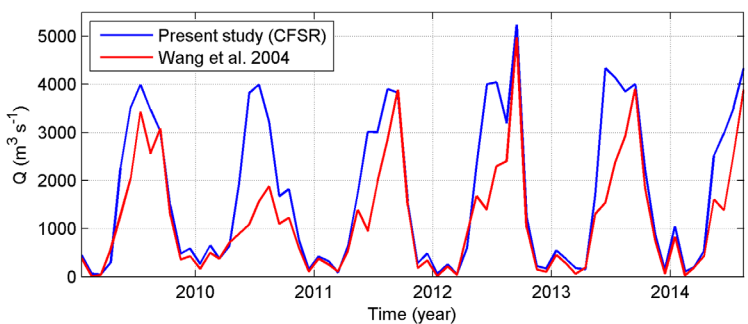


Figure 13. Modeled mean monthly discharge along the Prince William Sound coastline from January 2009 through August 2014.

elsewhere. First, many studies of ocean circulation use coarse resolution (0.5–1.0°; monthly climatology) freshwater inflow forcing [e.g., *Forget et al.*, 2015]. One example data product is the Global Composite Runoff Fields [*Fekete et al.*, 2002]. Figure 12 shows the mean annual runoff depth for the GOA region from this database. Gray cells indicate cells for which no runoff is available. This data set, which is based on the *Matsuura and Willmott* [2012a,b] reanalysis weather grids and a simple water balance model, yields an annual runoff into the GOA of only $440 \text{ km}^3 \text{ w.eq. yr}^{-1}$, which is far below the predictions of the present study. This error in boundary forcing will propagate through the oceanographic model to produce errors in water column properties and circulations. Additionally, the data set only reports climatologies of runoff and is therefore unable to predict interannual variability.

High spatial resolution alone is not enough to ensure accurate predictions of runoff, however. *Farrara et al.* [2013] and *Li et al.* [2013] conducted Regional Ocean Modeling System (ROMS) simulations of Prince William Sound, Alaska for the summer of 2009, during which time a comprehensive field campaign in the Sound took place. The ROMS simulations were forced with the 5 km runoff model of *Wang et al.* [2004] and it was observed (Figure 5 of *Farrara et al.* [2013] and *Li et al.* [2013]) that the ROMS salinities were much higher than the observations. Figure 13 shows a comparison of the mean monthly discharge into Prince William Sound from the *Wang et al.* [2004] model and the present CFSR-forced model. The Wang model underestimates summer runoff and has a mean annual runoff that is about 60% that of the present model. The higher freshwater discharge of the present model would serve to freshen the Sound and close the misfit between the observed and ROMS-simulated salinities. It is difficult to fully diagnose the underestimates of the Wang model, but candidates include different modeling strategies, different meteorological forcing, and different calibration approaches. *Wang et al.* [2004] used a temperature-index approach, NCEP reanalysis grids, and calibrated their model using the Copper River, which is a large interior river hydrologically very different from the glacierized coastal watersheds making up Prince William Sound.

6. Conclusions

This study applied a physically based energy balance model at a high spatiotemporal resolution to simulate the freshwater fluxes and glacier mass balance in the GOA. We found that the simulations, both at the local and regional scale, were influenced greatly by the selection of meteorological forcing, especially the precipitation and air temperature in the mountainous regions. These are regions with sparse observations, thus the meteorological forcing is highly dependent on the accuracy of the underlying weather model used in the reanalysis generation. Of the four weather products tested, the CFSR meteorological forcing performed the best in the simulation of regional FWD and GVL.

This study also partitioned the coastal freshwater runoff into its source components (rainfall, snow melt, ice melt) and demonstrated how the composition of coastal runoff varies seasonally. The high spatial resolution means that this partitioning can be done at the scale of individual fjords and bays along the Alaska coast,

Table A1. Default Model Parameters and Key Citations

Variable	Parameter Name	Default Value	Key Citation
n	Number of nearest stations used for interpolation	5	<i>Daly et al.</i> [2002]
L	Curvature length scale (m) used for wind model	500	<i>Liston</i> [1995]
ws_{min}	Minimum wind speed (m s^{-1})	1.0	<i>Liston and Elder</i> [2006a,b]
Γ	Monthly temperature lapse rate ($^{\circ}\text{C km}^{-1}$)	4.4–8.2	<i>Kunkel</i> [1989]
χ	Monthly precipitation adjustment factor (km^{-1})	0.2–0.35	<i>Thornton et al.</i> [1997]
$T_{rain/snow}$	Rain/snow threshold temperature ($^{\circ}\text{C}$)	2.0	<i>Auer</i> [1974]
g	Canopy gap fraction	0.2	<i>Liston and Elder</i> [2006a,b]
$\alpha_{s,fresh}$	Cloud fraction adjustment factor	1.0	<i>Liston and Elder</i> [2006a,b]
$\alpha_{s,melt-forest}$	Fresh, nonmelting snow albedo	0.80	<i>Mernild et al.</i> [2008]
$\alpha_{s,melt-clearing}$	Melting snow albedo, under forest canopy	0.45	<i>Liston and Elder</i> [2006a,b]
α_{ice}	Melting snow albedo, nonforested area	0.60	<i>Liston and Elder</i> [2006a,b]
ρ_{snow}	Bare glacier albedo, dry and melting	0.40	<i>Mernild et al.</i> [2008]
$V_{ice,sc}$	Initial snow density	300	<i>Liston</i> [1995]
$V_{ice,rf}$	Flow velocity (m s^{-1}) through snow-covered ice	0.12	<i>Liston and Mernild</i> [2012]
$V_{land,sc}$	Flow velocity (m s^{-1}) through snow-covered land	0.20	<i>Liston and Mernild</i> [2012]
$V_{land,rf}$	Flow velocity (m s^{-1}) through snow-free land	0.10	<i>Liston and Mernild</i> [2012]
		0.08	<i>Liston and Mernild</i> [2012]

helping to advance what is known about the ecology and biogeochemistry of Alaska nearshore waters. This study represents a major step forward in our understanding of the contribution of different source waters to the FWD, and how that is tied to GVL.

Finally, this study demonstrates the value and limitations of GRACE data in monitoring elements of the hydrosphere and cryosphere. The misfit between the annual amplitudes from the model and from GRACE indicates that high-resolution forward hydrological modeling is needed to continue to improve GRACE's ability to isolate changes in ice storage.

Appendix A

Appendix A contains Table A1, which lists the primary model parameters of MicroMet, SnowModel, and HydroFlow. The table lists the model parameter variables, names, default values, and key citations.

Acknowledgments

This work was supported primarily by a grant from the Oil Spill Recovery Institute (grant 12-10-07). J. Beamer thanks the Geophysical Institute, University of Alaska Fairbanks for hosting a visit in summer 2014 and the CUAHSI Pathfinder Fellowship for associated support. A. Arendt was also funded by NASA Cryospheric Sciences (grant NNX13AD52A), the Washington Research Foundation Fund for Innovation in Data-Intensive Discovery, and the Moore/Sloan Data Science Environments Project at the University of Washington. We would also like to thank Scott Luthcke and the NASA Goddard Space Geodesy Group for providing the GRACE data, Michael Hekkers at the University of Alaska, Southeast for collecting mass balance data on Mendenhall Glacier, Michael Loso for the Eklutna Glacier data, and Ed Neal and Eran Hood for assisting in selection of local domains. The data used for this project are available as follows: (i) Digital elevation model—<https://lta.cr.usgs.gov/HYDRO1K>; (ii) Land cover—<http://www.ccc.org/tools-and-resources/map-files/land-cover-2005/>; (iii) Randolph glacier cover—http://www.glims.org/RGI/rgi32_dl.html; (iv) Soils data—<http://www.fao.org/soils-portal/soil-survey/soil-maps-and-databases/harmonized-world-soil-database-v12/en/>; (v) NARR data—<ftp://ftp.cdc.noaa.gov/Datasets/NARR/monolevel/>; (vi) MERRA data—http://disc.sci.gsfc.nasa.gov/daac-bin/ftpSubset.pl?LOOKUPID_List=MA13CPASM; (vii) CFSR data—<http://rda.ucar.edu/datasets/ds093.0/>; (viii) Weather grids—<ftp://ftp.ncdc.noaa.gov/pub/data/griddednw-pac/>; (ix) GRACE Level-1B—<http://podaac.jpl.nasa.gov/datasetList?search=GRACE>; and (x) Streamflow—<http://waterdata.usgs.gov/nwis>. Sample model outputs (SWE and discharge grids) are available at <http://www.aoos.org/>.

References

- Abatzoglou, J. T. (2011), Development of gridded surface meteorological data for ecological applications and modelling, *Int. J. Climatol.*, 33, 121–131, doi:10.1002/joc.3413.
- Arendt, A., S. Luthcke, A. Gardner, S. O'Neil, D. Hill, G. Moholdt, W. Abdalati, and W. Abdalati (2013), Analysis of a GRACE global mascon solution for Gulf of Alaska glaciers, *J. Glaciol.*, 59, 913–924, doi:10.3189/2013JoG12J197.
- Auer, A. H. (1974), The rain versus snow threshold temperatures, *Weatherwise*, 27, 67, doi:10.1080/00431672.1974.9931684.
- Bieniek, P. A., et al. (2012), Climate divisions for Alaska based on objective methods, *J. Appl. Meteorol. Climatol.*, 51, 1276–1289, doi:1520-0442(1989)002/JAMC-D-11-0168.1.
- Bieniek, P. A., J. E. Walsh, R. L. Thoman, U. S. Bhatt (2014), Using climate divisions to analyze variations and trends in Alaska temperature and precipitation, *J. Clim.*, 27, 2800–2818, doi:1520-0442(1989)002/JCLI-D-13-00342.1.
- Boyce, E. S., R. J. Motyka, and M. Truffer (2007), Flotation and retreat of a lake-calving terminus, Mendenhall Glacier, southeast Alaska, USA, *J. Glaciol.*, 53, 211–224, doi:10.3189/172756507782202928.
- Cogley, J. G., et al. (2011), Glossary of glacier mass balance and related terms, *IHP-VII Tech. Doc. Hydrol.* 86, IACS Contrib. 2, U. N. Educ., Sci. and Cult. Organ. Int. Hydrol. Programme, Paris.
- Daly, C., R. P. Neilson, and D. L. Phillips (1994), A statistical-topographic model for mapping climatological precipitation over mountainous terrain, *J. Appl. Meteorol.*, 33, 140–158, doi:1520-0442(1989)002/1520-0450.
- Daly, C., W. P. Gibson, G. H. Taylor, G. L. Johnson, and P. Pasteris (2002), A knowledge-based approach to the statistical mapping of climate, *Clim. Res.*, 22, 99–113, doi:10.3354/crc022099.
- Daly, C., M. Halbleib, J. I. Smith, W. P. Gibson, M. K. Doggett, G. H. Taylor, J. Curtis, and P. P. Pasteris (2008), Physiographically sensitive mapping of climatological temperature and precipitation across the conterminous United States, *Int. J. Climatol.*, 28, 2031–2064, doi:10.1002/joc.1688.
- Elsberg, D. H., W. D. Harrison, K. A. Echelmeyer, and R. M. Kimmel (2001), Quantifying the effects of climate and surface change on glacier mass balance, *J. Glaciol.*, 47, 649–658, doi:10.3189/172756501781831783.
- Etherington, L. L., P. N. Hooge, E. R. Hooge, and D. F. Hill (2007), Oceanography of Glacier Bay, Alaska: Implications for biological patterns in a glacial fjord estuary, *Estuaries Coasts*, 30, 927–944.
- Farrara, J. D., et al. (2013), A data-assimilative ocean forecasting system for the Prince William Sound and an evaluation of its performance during Sound Predictions 2009, *Cont. Shelf Res.*, 63, S193–S208.
- Federer, C. A., C. Verosmarty, and B. Fekete (1996), Intercomparison of methods for calculating potential evaporation in regional and global water balance models, *Water Resour. Res.*, 32, 2315–232, doi:10.1029/96WR00801.
- Fekete, B., C. Vörösmarty, and W. Grabs (2002), Global composite runoff fields on observed river discharge and simulated water balances, Water Syst. Anal. Group, Univ. of N. H., and Global Runoff Data Cent., Fed. Inst. of Hydrol. (BfG), Koblenz, Germany.
- Fellman, J. B., R. G. M. Spencer, P. J. Hernes, R. T. Edwards, D. V. D'Amore, and E. Hood (2010), The impact of glacier runoff on the biodegradability and biochemical composition of terrigenous dissolved organic matter in near-shore marine ecosystems, *Mar. Chem.*, 121, 112–122, doi:10.1016/j.marchem.2010.03.009.
- Fellman, J. B., S. Nagorski, S. Pyare, A. W. Vermilyea, D. Scott, and E. Hood (2014), Stream temperature response to variable glacier coverage in coastal watersheds of Southeast Alaska, *Hydrol. Processes*, 28, 2062–2073, doi:10.1002/hyp.9742.
- Fellman, J. B., E. Hood, P. A. Raymond, J. Hudson, M. Bozeman, and M. Arimitsu (2015), Evidence for the assimilation of ancient glacier organic carbon in a proglacial stream food web, *Limnol. Oceanogr.*, 60, 1118–1128, doi:10.1002/lno.10088.
- Fischer, G., F. O. Nachtergaelie, S. Pryler, H. van Velthuizen, L. Verelst, and D. Wiberg (2008), *Global Agro-ecological Zones Assessment for Agriculture (GAEZ 2008)*, Int. Inst. for Appl. Syst. Anal., Luxenburg, Austria.
- Flint, L. E., A. L. Flint, J. H. Thorne, and R. Boynton (2013), Fine-scale hydrologic modeling for regional landscape applications: The California Basin Characterization Model development and performance, *Ecol. Processes*, 2(25), 1–21, doi:10.1186/2192-1709-2-25.
- Forget, G., J.-M. Campin, P. Heimbach, C. N. Hill, R. M. Ponte, and C. Wunsch (2015), ECCO version 4: An integrated framework for non-linear inverse modeling and global ocean state estimation, *Geosci. Model Dev.*, 8, 3071–3104.
- Fry, J. A., G. Xian, S. Jin, J. A. Dewitz, C. G. Homer, L. Yang, C. A. Barnes, N. D. Herold, and J. D. Wickham (2011), Completion of the 2006 national land cover database for the conterminous United States, *Photogramm. Eng. Remote Sens.*, 77, 858–864.
- Fuchs, T., J. Rapp, F. Rubel, and B. Rudolf (2001), Correction of synoptic precipitation observations due to systematic measuring errors with special regard to precipitation phases, *Phys. Chem. Earth Part B*, 26, 689–693, doi:10.1016/S1464-1909(01)00070-3.
- Hill, D. F., N. Bruhis, S. E. Calos, A. Arendt, and J. Beamer (2015), Spatial and temporal variability of freshwater discharge into the Gulf of Alaska, *J. Geophys. Res. Oceans*, 120, 634–646, doi:10.1002/2014JC010395.
- Hood, E., and L. Berner (2009), Effects of changing glacial coverage on the physical and biogeochemical properties of coastal streams in southeastern Alaska, *J. Geophys. Res.*, 114, G03001, doi:10.1029/2009JG000971.
- Hood, E., T. J. Battin, J. Fellman, S. O'Neil, and R. G. M. Spencer (2015), Storage and release of organic carbon from glaciers and ice sheets, *Nat. Geosci.*, 8, 91–96, doi:10.1038/ngeo2331.
- Huss, M., and R. Hock (2015), A new model for global glacier change and sea-level rise, *Front. Earth Sci.*, 3, 54, doi:10.3389/feart.2015.00054.

- Jackson, R. B., J. Canadell, J. R. Ehleringer, H. A. Mooney, O. E. Sala, and E. D. Schulze (1996), A global analysis of root distributions for terrestrial biomes, *Oecologia*, **108**, 389–411, doi:10.1007/BF00333714.
- Kane, D. L., and D. Yang (2004), Overview of water balance determinations for high latitude watersheds, in *Northern Research Basins Water Balance*, IAHS Publ., **290**, edited by D. L. Kane and D. Yang, (Proc. Workshop, Victoria, Canada, March), pp. 228–240, IAHS Press, Wallingford, U. K.
- Kienholz, C., S. Herreid, J. L. Rich, A. A. Arendt, R. Hock, and E. W. Burgess (2015), Derivation and analysis of a complete modern-date glacier inventory for Alaska and northwest Canada, *J. Glaciol.*, **61**(227), 403–420, doi:10.3189/2015JoG14J230.
- Kunkel, K. E. (1989), Simple procedures for extrapolation of humidity variables in the mountainous western United States, *J. Clim.*, **2**, 656–669, doi:10.1175/1520-0442(1989)002<0656:SPFEOH>2.0.CO;2.
- Larsen, C. F., E. Burgess, A. A. Arendt, S. O'Neal, A. J. Johnson, and C. Kienholz (2015), Surface melt dominates Alaska glacier mass balance, *Geophys. Res. Lett.*, **42**, 5902–5908, doi:10.1002/2015GL064349.
- Lader, R., U. S. Bhatt, J. E. Walsh, T. S. Rupp, and P. A. Bieniek (2016), Two-meter temperature and precipitation from atmospheric reanalysis evaluated for Alaska, *J. Appl. Meteorol. Climatol.*, **55**, 901–922, doi:10.1175/JAMC-D-15-0162.1.
- Lenaerts, J. T. M., J. H. van Angelen, M. R. van den Broeke, A. S. Gardner, B. Wouters, and E. van Meijgaard (2013), Irreversible mass loss of Canadian Arctic Archipelago glaciers, *Geophys. Res. Lett.*, **40**, 870–874, doi:10.1002/grl.50214.
- Li, Z., Y. Chao, J. Farrara, and J. McWilliams (2013), Impacts of distinct observations during the 2009 Prince William Sound field experiment: A data assimilation study, *Cont. Shelf Res.*, **63**, S209–S222.
- Lisi, P. J., D. E. Schindler, K. T. Bentley, and G. R. Pess (2013), Association between geomorphic attributes of watersheds, water temperature, and salmon spawn timing in Alaskan streams, *Geomorphology*, **185**, 78–86, doi:10.1016/j.geomorph.2012.12.013.
- Liston, G. E. (1995), Local advection of momentum, heat, and moisture during the melt of patchy snow covers, *J. Appl. Meteorol.*, **34**, 1705–1715, doi:10.1175/1520-0450-34.7.1705.
- Liston, G. E., and K. Elder (2006a), A meteorological distribution system for high-resolution terrestrial modeling (MicroMet), *J. Hydrometeorol.*, **7**, 217–234, doi:10.1175/JHM486.1.
- Liston, G. E., and K. Elder (2006b), A distributed snow-evolution modeling system (SnowModel), *J. Hydrometeorol.*, **7**, 1259–1276, doi:10.1175/JHM548.1.
- Liston, G. E., and C. A. Hiemstra (2011), The changing cryosphere: Pan-Arctic snow trends (1979–2009), *J. Clim.*, **24**, 5691–5712, doi:10.1175/JCLI-D-11-00081.1.
- Liston, G. E., and S. H. Mernild (2012), Greenland freshwater runoff. Part I: A runoff routing model for glaciated and nonglaciated landscapes (HydroFlow), *J. Clim.*, **25**, 5997–6014, doi:10.1175/JCLI-D-11-00591.1.
- Loso, M. J. (2011), The diminishing role of glacier runoff into Eklutna Lake: Potential impacts on hydropower and water supply for the Municipality of Anchorage, *Final Rep. Natl. Inst. Water Resour. 2010AK87B*, NIWR Funded Res. Proj., Alaska Pac. Univ., Anchorage, Alaska.
- Luthcke, S. B., T. J. Sabaka, B. D. Loomis, A. A. Arendt, J. J. McCarthy, and J. Camp (2013), Antarctica, Greenland and Gulf of Alaska land-ice evolution from an iterated GRACE global mascon solution, *J. Glaciol.*, **59**, 613–631, doi:10.3189/2013JoG12J147.
- Matsuura, K., and C. J. Willmott (2012a), *Terrestrial Air Temperature: 1900–2010 Gridded Monthly Time Series (version 3.01)*. [Available at <http://climate.geog.udel.edu/climate/>.]
- Matsuura, K., and C. J. Willmott (2012b), *Terrestrial Precipitation: 1900–2010 Gridded Monthly Time Series (version 3.02)*. [Available at <http://climate.geog.udel.edu/climate/>.]
- McAfee, S. A., G. Guentchev, and J. K. Eischeid (2013), Reconciling precipitation trends in Alaska: 1. Station-based analyses, *J. Geophys. Res. Atmos.*, **118**, 7523–7541, doi:10.1002/jgrd.50572.
- McGrath, D., L. Sass, S. O'Neal, A. Arendt, G. Wolken, A. Gusmeroli, C. Kienholz, and C. McNeil (2015), End-of-winter snow depth variability on glaciers in Alaska, *J. Geophys. Res. Earth Surf.*, **120**, 1530–1550, doi:10.1002/2015JF003539.
- McNabb, R. W., R. Hock, and M. Huss (2015), Variations in Alaska tidewater glacier frontal ablation, 1985–2013, *J. Geophys. Res. Earth Surf.*, **120**, 120–136, doi:10.1002/2014JF003276.
- Melloh, R. A., J. P. Hardy, R. E. Davis, and P. B. Robinson (2001), Spectral albedo/reflectance of littered forest snow during the melt season, *Hydro. Processes*, **15**, 3409–3422, doi:10.1002/hyp.1043.
- Mernild, S. H., and G. E. Liston (2012), Greenland freshwater runoff. Part II: Distribution and trends, 1960–2010, *J. Clim.*, **25**, 6015–6035, doi:10.1175/JCLI-D-11-00592.1.
- Mernild, S. H., G. E. Liston, B. Hasholt, and N. T. Knudsen (2006), Snow distribution and melt modeling for Mittivakkat Glacier, Ammassalik Island, Southeast Greenland, *J. Hydrometeorol.*, **7**, 808–824, doi:10.1175/JHM522.1.
- Mernild, S. H., G. E. Liston, C. A. Hiemstra, and K. Steffen (2008), Surface melt area and water balance modeling on the Greenland Ice Sheet 1995–2005, *J. Hydrometeorol.*, **9**, 1191–1211, doi:10.1175/2008JHM957.1.
- Mernild, S. H., T. L. Mote, and G. E. Liston (2011), Greenland ice sheet surface melt extent and trends: 1960–2010, *J. Glaciol.*, **57**, 621–628.
- Mernild, S. H., G. E. Liston, and C. A. Hiemstra (2014), Northern hemisphere glacier and ice cap surface mass balance and contribution to sea level rise, *J. Clim.*, **27**, 6051–6073, doi:10.1175/JCLI-D-13-00669.1.
- Mesinger, F., et al. (2006), North American regional reanalysis, *Bull. Am. Meteorol. Soc.*, **87**, 343–360, doi:10.1175/BAMS-87-3-343.
- Molnia, B. F. (2008), Glaciers of North America: Glaciers of Alaska, in *Satellite Image Atlas of Glaciers of the World*, edited by R. S. Williams Jr., and J. G. Ferrigno, U.S. Geol. Surv. Prof. Pap., **1386-K**, 525 pp.
- Neal, E. G., E. Hood, and K. Smikrud (2010), Contribution of glacier runoff to freshwater discharge into the Gulf of Alaska, *Geophys. Res. Lett.*, **37**, L06404, doi:10.1029/2010GL042385.
- O'Neal, S., E. Hood, A. Arendt, and L. Sass (2014), Assessing streamflow sensitivity to variations in glacier mass balance, *Clim. Change*, **123**, 329–341, doi:10.1007/s10584-013-1042-7.
- O'Neal, S., et al. (2015), Icefield-to-Ocean linkages across the northern pacific coastal temperate rainforest ecosystem, *BioScience*, biv027, doi:10.1093/biosci/biv027.
- Østrem, G., and M. Brugmann (1991), *Glacier Mass-Balance Measurements, A Manual for Field and Office Work*, NHRI Sci. Rep. **4**, 224 pp., Norw. Water Resour. and Energy Dir., Oslo.
- Pfeffer, W. T., et al. (2014), The Randolph Glacier Inventory: A globally complete inventory of glaciers, *J. Glaciol.*, **60**, 537–552, doi:10.3189/2014JoG13J176.
- Priestley, C. H. B., and R. J. Taylor (1972), On the assessment of surface heat flux and evaporation using large-scale parameters, *Mon. Weather Rev.*, **100**, 81–92, doi:10.1175/1520-0493(1972)100<0081:OTAOSH>2.3.CO;2.
- Radić, V., and R. Hock (2013), Glaciers in the earth's hydrological cycle: Assessments of glacier mass and runoff changes on global and regional scales, *Surv. Geophys.*, **35**, 813–837, doi:10.1007/s10712-013-9262-y.
- Ragettli, S., and F. Pellicciotti (2012), Calibration of a physically based, spatially distributed hydrological model in a glacierized basin: On the use of knowledge from glaciometeorological processes to constrain model parameters, *Water Resour. Res.*, **48**, W03509, doi:10.1029/2011WR010559.

- Reid, T. D., and B. W. Brock (2010), An energy-balance model for debris-covered glaciers including heat conduction through the debris layer, *J. Glaciol.*, 56, 903–916.
- Rienecker, M. M., et al. (2011), MERRA: NASA's modern-era retrospective analysis for research and applications, *J. Clim.*, 24, 3624–3648, doi: 10.1175/JCLI-D-11-00015.1.
- Rodell, M., et al. (2004), The global land data assimilation system, *Bull. Am. Meteorol. Soc.*, 85, 381–394, doi:10.1175/BAMS-85-3-381.
- Royer, T. C. (1982), Coastal fresh water discharge in the northeast Pacific, *J. Geophys. Res.*, 87, 2017–2021, doi:10.1029/JC087iC03p02017.
- Saha, S., et al. (2010), The NCEP climate forecast system reanalysis, *Bull. Am. Meteorol. Soc.*, 91, 1015–1057, doi:10.1175/2010BAMS3001.1.
- Sass, L. C. (2011), Characterizing Eklutna Glacier's response to climate through measurements of mass balance, geometry, and motion, MSc thesis, Alaska Pac. Univ., Dep. of Environ. Sci., Anchorage, Alaska.
- Schaap, M. G., F. J. Leij, and M. T. van Genuchten (2001), Rosetta: A computer program for estimating soil hydraulic parameters with hierarchical pedotransfer functions, *J. Hydrol.*, 251, 163–176, doi:10.1016/S0022-1694(01)00466-8.
- Schnorbus, M., A. Werner, and K. Bennett (2014), Impacts of climate change in three hydrologic regimes in British Columbia, Canada, *Hydrolog. Processes*, 28, 1170–1189, doi:10.1002/hyp.9661.
- Shuttleworth, W. J. (2007), Putting the 'vap' into evaporation, *Hydrolog. Earth Syst. Sci.*, 11, 210–244, doi:10.5194/hess-11-210-2007.
- Singer, G. A., C. Fasching, L. Wilhelm, J. Niggemann, P. Steier, T. Dittmar, and T. J. Battin (2012), Biogeochemically diverse organic matter in Alpine glaciers and its downstream fate, *Nat. Geosci.*, 5, 710–714, doi:10.1038/ngeo1581.
- Thornton, P. E., S. W. Running, and M. A. White (1997), Generating surfaces of daily meteorological variables over large regions of complex terrain, *J. Hydrol.*, 190, 214–251, doi:10.1016/S0022-1694(96)03128-9.
- University of Alaska Southeast (2015), Mass Balance Data for Mendenhall Glacier, 2006–2012, Environ. Sci. Program., Juneau, Alaska.
- Van Beusekom, A. E., S. R. O'Neil, R. S. March, L. C. Sas, and L. H. Cox (2010), Re-analysis of Alaskan benchmark glacier mass-balance data using the index method, *U.S. Geol. Surv. Sci. Invest. Rep.* 2010–5247, 16 pp.
- Wang, J., M. Jin, D. L. Musgrave, and M. Ikeda (2004), A hydrological digital elevation model for freshwater discharge into the Gulf of Alaska, *J. Geophys. Res.*, 109, C07009, doi:10.1029/2002JC001430.
- Weingartner, T. J., S. L. Danielson, and T. C. Royer (2005), Freshwater variability and predictability in the Alaska Coastal Current, *Deep Sea Res., Part II*, 52, 169–191, doi:10.1016/j.dsr2.2004.09.030.